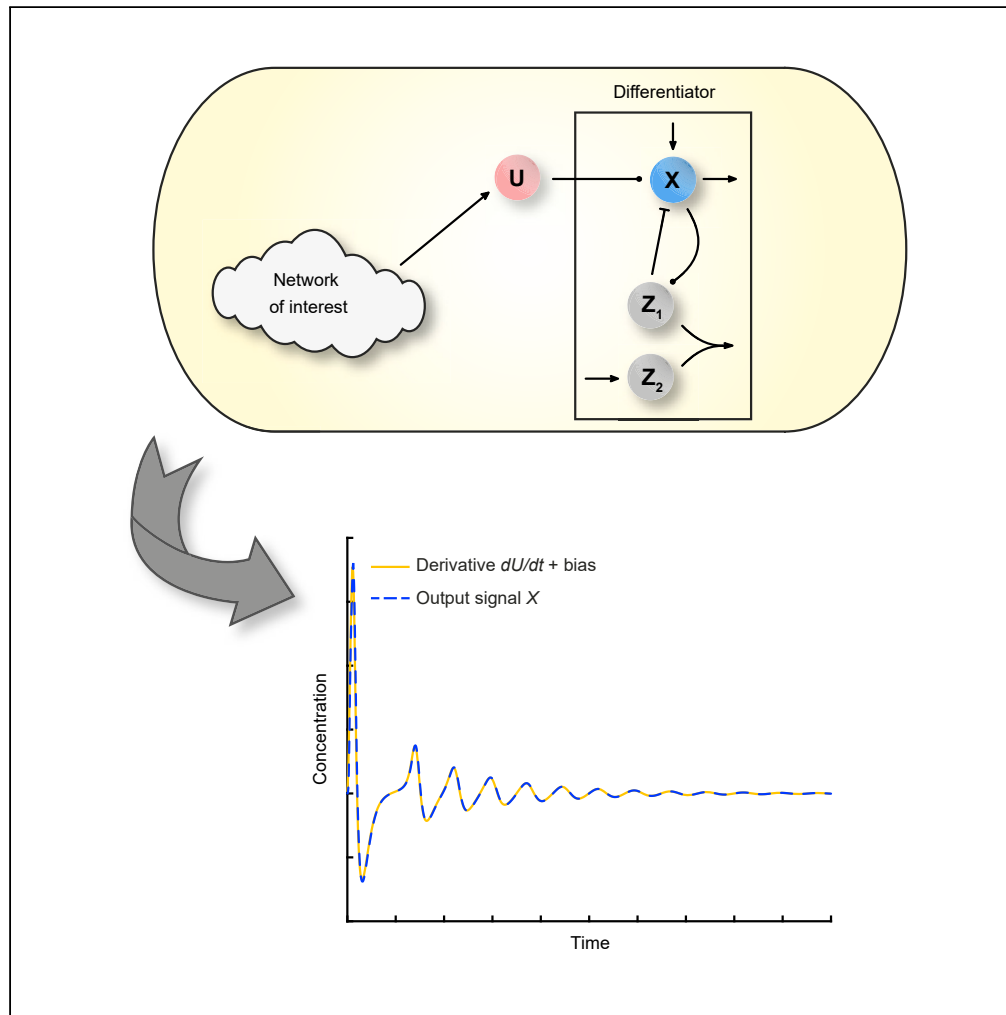


Article

Biomolecular mechanisms for signal differentiation



Emmanouil Alexis,
Carolin C.M.
Schulte, Luca
Cardelli, Antonis
Papachristodoulou

antonis@eng.ox.ac.uk

Highlights

Calculating the speed or higher derivatives of molecular signals has been a challenge

Biomolecular topologies acting as signal differentiators are studied

High performance and insensitivity to high-frequency input signals can be achieved

Natural circuits and synthetic realizations for signal differentiation are described

Alexis et al., iScience 24,
103462
December 17, 2021 © 2021
<https://doi.org/10.1016/j.isci.2021.103462>

Article

Biomolecular mechanisms for signal differentiation

Emmanouil Alexis,¹ Carolin C.M. Schulte,^{1,2} Luca Cardelli,³ and Antonis Papachristodoulou^{1,4,*}

SUMMARY

Cells can sense temporal changes of molecular signals, allowing them to predict environmental variations and modulate their behavior. This paper elucidates biomolecular mechanisms of time derivative computation, facilitating the design of reliable synthetic differentiator devices for a variety of applications, ultimately expanding our understanding of cell behavior. In particular, we describe and analyze three alternative biomolecular topologies that are able to work as signal differentiators to input signals around their nominal operation. We propose strategies to preserve their performance even in the presence of high-frequency input signal components which are detrimental to the performance of most differentiators. We find that the core of the proposed topologies appears in natural regulatory networks and we further discuss their biological relevance. The simple structure of our designs makes them promising tools for realizing derivative control action in synthetic biology.

INTRODUCTION

Measuring the speed at which a physical process evolves over time is of central importance to science and engineering. This can be done by computing the time derivative of the function describing the process. Several examples of cellular systems exhibiting derivative action indicate that calculating the rate of change of biological processes is essential in nature. The retina of our eyes, for instance, is one of the best-studied neural networks of the brain. Its response to changes in light intensity reveals typical characteristics of derivative action which stem from the interaction between cone and horizontal cells (Wilson, 1999; Åström and Murray, 2021). In microbiology, the chemotaxis signaling pathway in bacteria such as *Escherichia coli* involves computation of time derivatives: To navigate toward nutrients and away from toxins, bacteria are able to sample their environment as they move and convert spatial gradients into temporal ones (Alon, 2019; Shimizu et al., 2010; Iglesias and Devreotes, 2008; Barkai and Leibler, 1997; Block et al., 1983; Macnab and Koshland, 1972). Furthermore, in the context of cellular energy metabolism, *in silico* studies have revealed the role of creatine phosphate as a buffering species that allows for adaptation to a changing demand of adenosine triphosphate (ATP), thus exploiting the anticipatory action enabled by derivative control (Cloutier and Wellstead, 2010). This observation is a specific example of a broader class of biomolecular processes where the presence of rapid buffering proves to be equivalent to negative derivative feedback (Hancock et al., 2017).

In traditional engineering, differentiators refer to devices capable of applying time differentiation to an input stimulus, for example a mechanical or electrical signal. In the rapidly growing field of synthetic biology, the ability to build reliable biomolecular differentiators would offer considerable advantages (Steel et al., 2017; Del Vecchio et al., 2016; Lu et al., 2009). As an immediate application, such genetic circuits would be able to track the rate of change of the concentration of biomolecules, thus acting as speed biosensors. This is of interest when assessing uptake rates of certain molecules, such as uptake of pollutants into bacteria used for bioremediation (Chen and Wilson, 1997; Pieper and Reineke, 2000). They can also allow for advanced regulation strategies in the cellular environment by enabling the construction of more efficient bio-controllers, e.g., Proportional-Integral-Derivative (PID) control schemes, the workhorses of modern technological process control applications (Åström and Murray, 2021). In general, derivative control can enhance the stability of a feedback system and provide a smoother transient response.

Recent efforts in this rather underexplored research area include the design of a differentiator module consisting of linear input/output functions realized by specific processes of protein production (Halter et al., 2017; Halter et al., 2019). It has further been demonstrated that calculation of time derivatives is possible by using ultrasensitive topologies operating within a negative feedback loop (Samaniago et al., 2019), and a motif capable of computing positive and negative temporal gradients, which includes input delays and

¹Department of Engineering Science, University of Oxford, Oxford OX1 3PJ, UK

²Department of Plant Sciences, University of Oxford, Oxford OX1 3RB, UK

³Department of Computer Science, University of Oxford, Oxford OX1 3QD, UK

⁴Lead contact

*Correspondence: antonis@eng.ox.ac.uk

<https://doi.org/10.1016/j.isci.2021.103462>



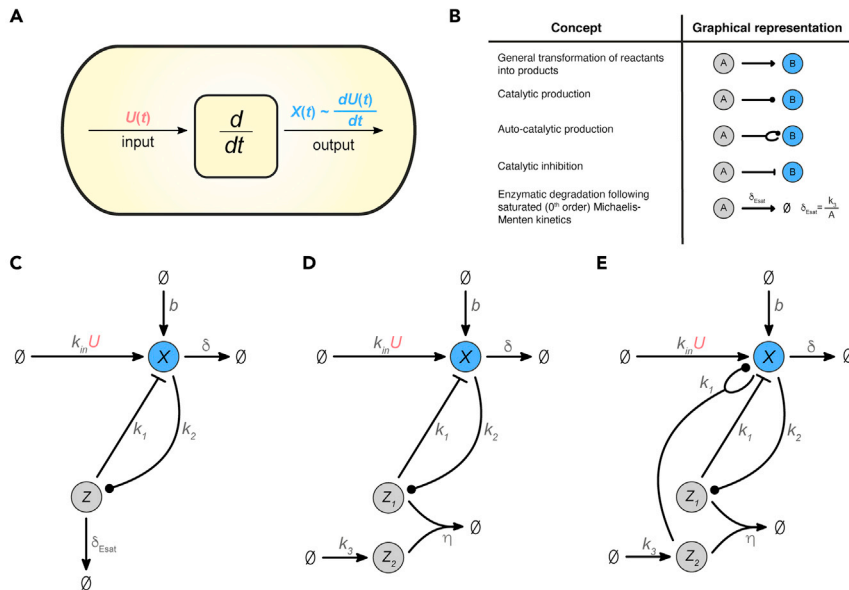


Figure 1. Biomolecular structures capable of signal differentiation

(A) Schematic representation of the notion of signal differentiation carried out by a biomolecular device inside the cell. (B) Graphical representation of the biological concepts found in the signal differentiator motifs. To describe the different kind of biomolecular reactions the following notation is adopted: (\rightarrow) means that the transformation of reactants into products only happens in the direction of the arrow. ($\xrightarrow{\cdot}$) indicates that reactants enable product formation without being consumed. (\dashv) denotes inhibition of products by a reactant where the reactant is not consumed. In addition, the depicted concept of enzymatic degradation is further analyzed in [STAR Methods Equilibria and stability of biomolecular signal differentiators: Biomolecular Signal Differentiator-I](#).

(C) Topology of Biomolecular Signal Differentiator - I or BioSD-I ([Equation \(1\)](#)).

(D) Topology of Biomolecular Signal Differentiator - II or BioSD-II ([Equation \(2\)](#)).

(E) Topology of Biomolecular Signal Differentiator - III or BioSD-III ([Equation \(3\)](#)).

the idea of an incoherent feedforward loop, has been presented ([Samaniego et al., 2020](#)). With the aim of providing derivative action in PID control architectures, networks directly inspired by bacterial chemotaxis ([Chevalier et al., 2019](#)) or based on the so-called dual rail encoding have also been proposed ([Whitby et al., 2021](#); [Paulino et al., 2019](#)). This approach enables the representation of both positive and negative signals via biomolecular species by decomposing a signal into two non-negative parts ([Oishi and Klavins, 2011](#)). Finally, a derivative controller tailored to gene expression is analyzed in ([Modi et al., 2019](#)), while in the PID architecture introduced in ([Filo and Khammash, 2021](#)), derivative control is carried out with inseparable connection to proportional and integral actions.

In this article, we introduce novel differentiator modules aiming to elucidate unexplored mechanisms that cells potentially exploit to achieve signal differentiation. In parallel, these motifs can pave the way for designing efficient and reliable synthetic signal differentiator devices in a cellular context. Notably, our motifs offer considerable ease of experimental implementation compared to some of the earlier discussed designs which are based on more “artificial” mechanisms such as dual-rail encoding. In addition, the motifs under consideration can function as independent, general-purpose differentiators, which may be a challenging task for other topologies, such as some control-oriented topologies showing derivative action. Moreover, under suitable tuning high accuracy of temporal derivative calculation for a wide range of molecular signals can be guaranteed.

Specifically, we present three biomolecular architectures capable of functioning as signal differentiators around their equilibria. We call them Biomolecular Signal Differentiators (BioSD). Each of these networks can be interpreted as a modular and tunable topology inside the cell that accepts a molecular signal as an input and produces an output signal proportional to the time derivative of the input signal ([Figure 1A](#)). The output corresponds to a biochemical species whose concentration can be measured. The proposed architectures provide simple blueprints for the design of synthetic biomolecular differentiators, but can also be interpreted as lenses through which derivative action in natural systems can be identified and studied.

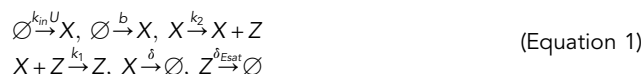
We demonstrate the special characteristics and the performance trade-offs of the three BioSD architectures (BioSD-I, II, and III) via theoretical analyses and numerical simulations. We also discuss a major obstacle of both technological and biological differentiators, namely amplification of undesired high-frequency components of the input signal, and propose strategies to overcome this obstacle. Finally, we show the occurrence of one of the BioSD topologies in natural regulatory networks involved in bacterial adaptation to stress conditions and present potential synthetic implementations for all three topologies, highlighting the biological relevance of our designs.

RESULTS

Biological structure

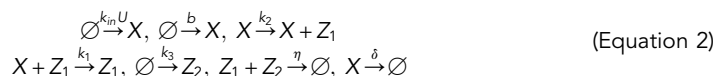
We begin by presenting the molecular interactions in the BioSD circuits as chemical reaction networks (CRNs). These circuits represent three alternative topological entities which, under certain assumptions, realize the same concept of signal differentiation. In the analysis that follows, the input and output signals of the differentiators are generally treated as biomolecular species, namely U and X respectively. Nevertheless, an input signal may also refer to different concepts such as light, temperature or pH.

Figure 1C illustrates the first architecture, BioSD-I, which consists of the following reactions:

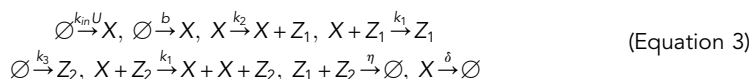


Here, the production of output species X depends on two reactions. One of them has a constant rate while the other occurs at a rate proportional to the concentration of input species U . It is convenient to represent such processes via reactions of the form $\emptyset \xrightarrow{r} X$, where r can be a constant or a time-varying quantity, e.g., biomolecular concentration. This allows us to describe general concepts of production without the need to specify their impact on the reactants involved. Furthermore, X also catalyzes the formation of species Z which, in turn, inhibits X . Note that the process of inhibition is interpreted as catalysis of degradation. Finally, the removal rate of X is proportional to its concentration (first-order decay) while, as indicated by the notation δ_{Esat} (defined in Figure 1B), Z adheres to a constant rate of decay (0th-order decay). The latter behavior is attained through enzyme-catalyzed degradation of Z where the enzyme is operating at saturating substrate levels (for more details see [STAR Methods Equilibria and stability of biomolecular signal differentiators: biomolecular signal differentiator-I](#)).

In the second architecture, BioSD-II (Figure 1D), the formation process of output species X is the same as in BioSD-I, while Z_1 , the production of which is facilitated by X , and Z_2 annihilate each other. Z_1 inhibits X which decays in the same way as in BioSD-I. The reactions that form the corresponding CRN are:



Finally, Figure 1E shows the third topology, BioSD-III, which is described by the reactions:



This CRN includes an autocatalytic-like reaction: X is able to produce more of itself in the presence of Z_2 . The rest of its structure is identical to the CRN of BioSD-II.

Mathematical description

We now derive the dynamics of the proposed BioSD networks using the law of mass action (Del Vecchio and Murray, 2015) unless otherwise stated, adopting the same order of presentation as in the preceding section.

BioSD-I (CRN given by Equation (1)) can be described by the following system of Ordinary Differential Equations (ODEs):

$$\dot{X} = k_m U + b - k_1 XZ - \delta X \quad (\text{Equation 4a})$$

$$\dot{Z} = k_2 X - k_3 \quad (\text{Equation 4b})$$

Note that the enzymatic degradation of Z is assumed to follow saturated (0th-order) Michaelis-Menten kinetics, as previously discussed.

Next, from the CRN given by Equation (2) we obtain the following ODE model for BioSD-II:

$$\dot{X} = k_{in}U + b - k_1XZ_1 - \delta X \quad (\text{Equation 5a})$$

$$\dot{Z}_1 = k_2X - \eta Z_1Z_2 \quad (\text{Equation 5b})$$

$$\dot{Z}_2 = k_3 - \eta Z_1Z_2 \quad (\text{Equation 5c})$$

For the last circuit, BioSD-III, the CRN given by Equation (3) can be modeled using the following ODEs:

$$\dot{X} = k_{in}U + b - k_1XZ_1 + k_1XZ_2 - \delta X \quad (\text{Equation 6a})$$

$$\dot{Z}_1 = k_2X - \eta Z_1Z_2 \quad (\text{Equation 6b})$$

$$\dot{Z}_2 = k_3 - \eta Z_1Z_2 \quad (\text{Equation 6c})$$

By assuming a constant input U^* and setting the derivatives to zero, we can show that each of the BioSD network models has a unique equilibrium. In addition, we can prove through linearization that the equilibrium is locally exponentially stable (a detailed analysis can be found in [STAR Methods Equilibria and stability of biomolecular signal differentiators](#)). Near their steady-states, the circuits are able to exhibit derivative action, as shown in the next section. Furthermore, for the purpose of this study we assume that the parameter η in BioSD-II is sufficiently large which can lead to a practically insignificant concentration of species Z_2 (more details can be found in [STAR Methods The notion of strong rate of annihilation between \$Z_1\$, \$Z_2\$ \(large \$\eta\$ \) in biomolecular signal differentiator-II](#)). This constraint does not have to hold for BioSD-III, which includes the same annihilation reaction. Finally, Equations (5b) and (5c) indicate that in case $\dot{Z}_2 \approx 0$, the removal rate of Z_1 is roughly constant and equal to k_3 , similar to the 0th-order removal of Z in BioSD-I.

Achieving biological signal differentiation

In order for the proposed biomolecular modules to work as signal differentiators, we desire for their output X to be proportional to the derivative of their input U. This immediately raises the following challenge: Both U and X refer to biomolecular species concentrations and, by extension, represent non-negative signals. However, in the general case, the derivative of a nonnegative signal can take negative values and, as a result, X would need to go below zero. Thus, it could be argued that X is unable to express the rate of change of an arbitrary input signal. An obvious way to overcome this obstacle is to add a bias to the computed derivative. As we demonstrate here, the perfect candidate for realizing this bias is the steady state of X around which derivative action can be achieved.

We are interested in the local behavior of the BioSD networks and, therefore, consider input stimuli that do not force them to operate far away from their equilibrium. Subsequently, we assume that every input signal can be described as:

$$U = U^* + U^{TV} \quad (\text{Equation 7})$$

where U^* is constant while U^{TV} is time-varying. Here, we focus on Fourier transformable signals which is typically the case for physical signals in practical applications (for more details see [STAR Methods Signals under consideration](#)).

By linearizing and applying appropriate transformations, we can show that the dynamics of the output of any of the three BioSD topologies presented in the previous section can be approximated by the following non-dimensional second - order differential equation (see [STAR Methods Behavior analysis of biomolecular signal differentiators](#)):

$$\epsilon \ddot{x}_n + \epsilon \dot{x}_n + x_n = \dot{u}_n \quad (\text{Equation 8})$$

where x_n and u_n refer to the output and input, respectively and:

$$\epsilon = \frac{k_2^2}{k_1 k_3} (k_{in}U^* + b)^2 \quad (\text{Equation 9})$$

Equation (8) represents a signal differentiator accompanied with some filtering action. Indeed, the input/output relation in the Laplace domain can be described by the following transfer function (Oppenheim et al., 1996):

$$\tilde{\Delta}_{BSD}(s) = \frac{\tilde{X}_n(s)}{\tilde{U}_n(s)} = \frac{s}{\varepsilon(s^2 + s) + 1} \quad (\text{Equation 10})$$

where $\tilde{X}_n(s)$ and $\tilde{U}_n(s)$ are the Laplace transform of the output x_n and input u_n , respectively and s is the Laplace variable (complex frequency). As can be seen from Equation (10), a BioSD network is the series combination of an ideal differentiator and a second-order low pass filter (Samoilov et al., 2002). Therefore, for a given positive ε , the accuracy of signal differentiation depends on the frequency spectrum of the input signal or, in other words, the range of frequencies contained by it (see STAR Methods Signals under consideration). Accompanying a differentiator with a low-pass filter is a widely used strategy in traditional engineering in order to deal with high-frequency input noise (this topic is analyzed in Response to input signals corrupted by high-frequency noise and A structural addition for enhanced performance).

To gain a deeper insight, we calculate the Fourier transform (Oppenheim et al., 1996) of the output:

$$\tilde{X}_n(j\omega) = \tilde{\Delta}_{BSD}(j\omega)\tilde{U}_n(j\omega) \quad (\text{Equation 11})$$

where ω represents the frequency, j is the imaginary unit number ($j = \sqrt{-1}$) and $\tilde{X}_n(j\omega)$, $\tilde{U}_n(j\omega)$ are the Fourier transform of the output x_n and input u_n , respectively. Furthermore, $\tilde{\Delta}_{BSD}(j\omega)$ is the Fourier transform of the system's impulse response, also known as the frequency response of the system. (ibid.). Since we have a linear, asymptotically stable, system we can compute the latter Fourier transform from Equation (10) by setting $s = j\omega$. Thus, we have:

$$\tilde{X}_n(j\omega) = \frac{j\omega}{\varepsilon(-\omega^2 + j\omega) + 1}\tilde{U}_n(j\omega) \quad (\text{Equation 12})$$

The operation of (ideal) differentiation in the frequency domain is defined as:

$$\tilde{X}_{nd}(j\omega) = j\omega\tilde{U}_n(j\omega) \quad (\text{Equation 13})$$

To compare the output of an ideal differentiator to the one of a BioSD device, we introduce the following performance metric:

$$\tilde{\Lambda}(j\omega) = \frac{\tilde{X}_n(j\omega)}{\tilde{X}_{nd}(j\omega)} = \frac{1}{\varepsilon(-\omega^2 + j\omega) + 1} \quad (\text{Equation 14})$$

Using the magnitude-phase representation of Equation (14) we get:

$$|\tilde{\Lambda}(j\omega)| = \frac{1}{\sqrt{\varepsilon^2\omega^2 + (1 - \varepsilon\omega^2)^2}} \quad (\text{Equation 15})$$

and

$$\angle \tilde{\Lambda}(j\omega) = \arctan\left(\frac{-\varepsilon\omega}{1 - \varepsilon\omega^2}\right)$$

Signal differentiation of high accuracy is carried out when $|\tilde{\Lambda}(j\omega)|$ is close to $1 \angle 0^\circ$. As shown in Figure 2, there is a "low-frequency" range where this is true, but as ε decreases the aforementioned range expands toward "higher frequencies". In the time domain this entails that for a given positive ε , a BioSD device can work as an accurate signal differentiator for sufficiently slow input signals and, in that case, the BioSD output can be approximated by (see STAR Methods Behavior analysis of biomolecular signal differentiators):

$$X = \frac{k_{in}}{k_1 k_3} \dot{U} + \frac{k_3}{k_2} U \quad (\text{Equation 16})$$

There is a family of input signals for which the BioSD topologies are able to provide accurate differentiation regardless of the exact value of ε (see STAR Methods Behavior analysis of biomolecular signal differentiators). More specifically, this holds for input signals for which the term U^{TV} in Equation (7) is of the form:

$$U^{TV} = \xi_1 e^{-\xi_3 t} + \xi_2 t, \quad (\text{Equation 17})$$

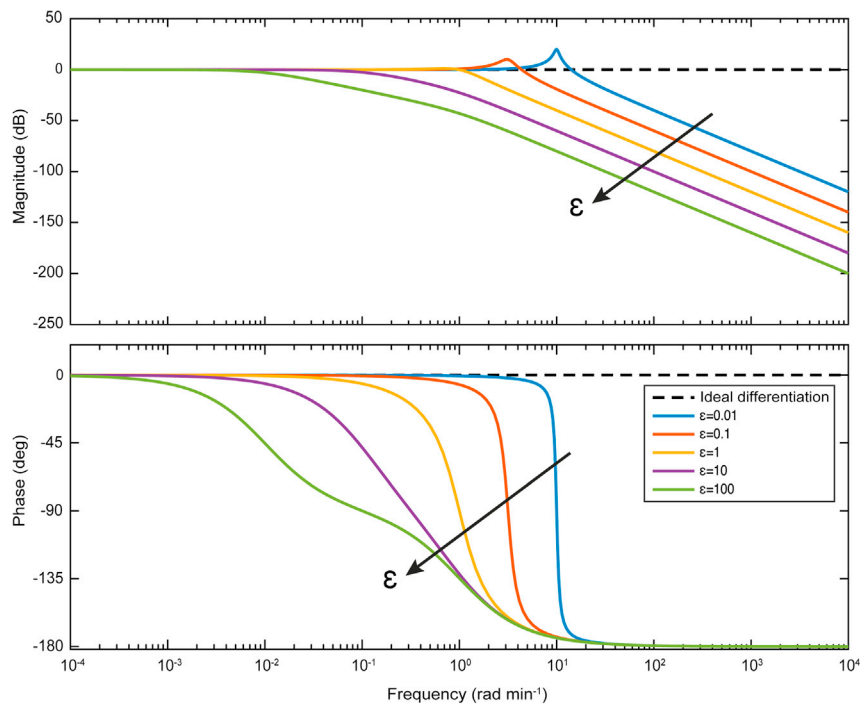


Figure 2. A performance metric for Biomolecular Signal Differentiators in the frequency domain

Bode plot of the metric given by Equation (14). Different colors represent the magnitude and the phase of the corresponding transfer function for different values of ϵ . The case of ideal differentiation corresponds to $\epsilon = 0$ and the direction in which the latter increases indicated by an arrow.

where ξ_1, ξ_2 are arbitrary constants and $\xi_3 = \frac{k_2}{k_3}(k_{in}U^* + b)$. If ξ_2 is not zero which implies linear growth over time, we assume that the above holds as long as the system stays near its equilibrium. This means that the term $\xi_2 t$ is sufficiently small. Indeed, several biological processes can generate (bounded) signals some part of which can be viewed as linear growth (Del Vecchio and Murray, 2015). We study such a scenario in Sensing the response speed of biomolecular networks.

As Equation (8) states, the response of a BioSD network, is given as the solution of a second-order non-homogeneous differential equation with constant coefficients where the forcing function is \dot{u}_n . The response can therefore be seen as the sum of two terms: a "transient" term which highly depends on the initial conditions and dies out with time; and a "steady-state" term which, under the conditions discussed above, can approximate the derivative of the input signal (Zill, 2012). Therefore, for input signals applied for a sufficiently long time, the BioSD output practically coincides with the latter since the effect of the former is negligible. However, this may not be always the case for short duration input signals where any undesired initial transient phenomena can greatly compromise the accuracy of the differentiator output.

From Equation (16), we can see that the BioSD modules use the biomolecular concentration $\frac{k_3}{k_2}$ as a bias. Around this point they can operate as signal differentiators, producing an output signal component which is proportional to the derivative of the input. The bias therefore depends only on two parameters which, ideally, can be adjusted as desired. This provides us with the freedom of choosing any (fixed) concentration of X as a bias, which will remain unchanged regardless of the rest of the model parameters, the input stimulus, or potential constant disturbances on the output. To appreciate this further, we recall the production reaction for X with constant rate b , which is included in each of the proposed CRNs. Besides its role as a structural requirement, this production reaction can also represent an external constant disturbance applied on X ; this, however, does not affect the zero-level we choose for our measurements. Once the concentration of X reaches this level, it will stay there until an input excitation appears and it will come back once the excitation stops. Hence, the previously mentioned fixed concentration can also be seen as a "rest position" for the differentiators.

The feature just described is of key importance and stems mainly from the following two sources: the stability that characterizes BioSDs and the fact that the steady-state of the output coincides with the aforementioned zero-level concentration. The latter is achieved due to integration carried out by the ‘memory’ function which is realized via species Z within BioSD-I and the quantity $Z_1 - Z_2$ within BioSD-II, III.

Tunability and accuracy

It is convenient for the circuit designer who aims to implement the BioSD topologies to be able to choose the parameter values and ensure that the resulting differentiators meet the expected performance requirements. Nonetheless, there may be cases where the number of system parameters that can be suitably tuned is limited, for instance due to constraints related to the cellular processes involved in the circuits under investigation. Even in this case, the architecture of our circuits allows for some tunability as long as the designer can choose some crucial parameters.

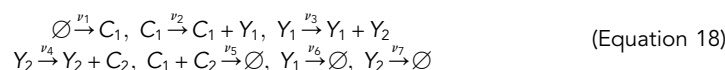
Consider for example the extreme scenario where only one of the model parameters can be regulated. If this parameter is k_3 , then, according to Equation (16), its appropriate tuning may result in an acceptable gain by which the output signal is multiplied (output gain) and bias based on which this signal is measured. At the same time, Equation (9) reveals that (contrary to other parameters) a small change in k_3 can affect ε significantly since the latter is inversely proportional to the cube of k_3 .

It immediately emerges from the above that the way we tune the BioSD networks defines the level of accuracy regarding their derivative action. Indeed, ε is subject to almost all parameter rates in these networks and, as pointed out in the previous section, the value of ε defines the range of frequencies over which BioSDs can accurately compute the rate of change of a biological signal.

Sensing the response speed of biomolecular networks

We now demonstrate through an example the ability of BioSD modules to compute the temporal derivative of biological signals. At the same time, we highlight one of their potential applications discussed above, namely as rate-of-change detectors or speed biosensors.

We consider the antithetic motif (Figure 3) (Briat, Gupta, and Khammash, 2016, 2018; Chevalier et al., 2019; Olsman et al., 2019a, 2019b; Olsman and Forni, 2020; Baetica et al., 2020):

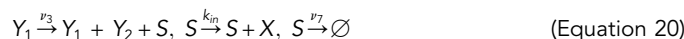


Species Y_1, Y_2 represent an arbitrary biological process whose output, Y_2 , can be robustly steered toward a desired value $\left(\frac{\nu_1}{\nu_4}\right)$. This is feasible through the feedback integral control which is implemented via species C_1, C_2 , thus achieving robust perfect adaptation. Depending on the parameter rates, the dynamics of the above architecture can be either stable or unstable. Nonetheless, even in a stable system, the species of interest, Y_2 , sometimes displays a long-lasting transient response with damped oscillations before it settles to a steady-state. This provides an opportunity to assess the ability of the BioSD networks to calculate the speed at which these oscillations evolve.

In order for a BioSD device to function as a biosensor for the CRN given by (Equation 18), a suitable interconnection between these circuits is required while preserving the modularity of the two networks and avoiding any loading problems, i.e., effects of retroactivity (Del Vecchio and Murray, 2015; Del Vecchio et al., 2008, 2016). One way to accomplish this is through the reaction:

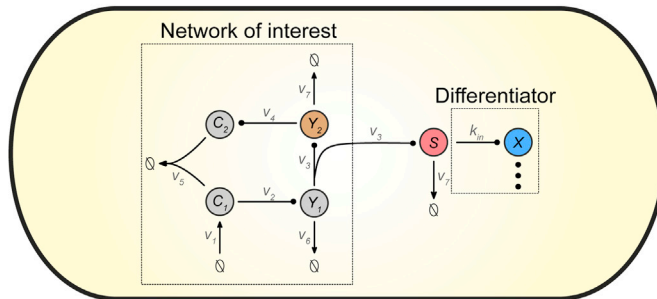


where Y_2 plays the role of the input species U without being consumed. Alternatively, in case the nature of Y_2 prevents it from directly producing X , we can use a separate sensory species S which is capable of participating in the formation of X . In particular, we assume that S is co-expressed with and decays at the same rate as Y_2 , i.e.:



Adopting the second interconnection as the most general one, we demonstrate in Figure 3 that the rate of change of the concentration of Y_2 can be accurately represented by the output of the BioSD networks. We also

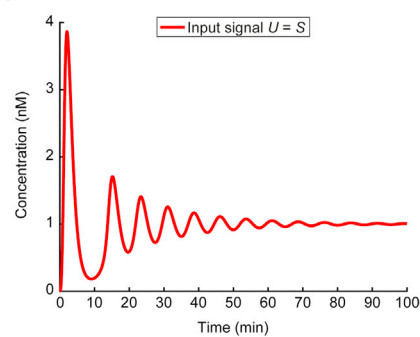
A



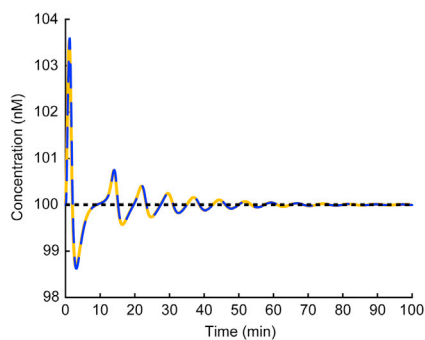
B

$$\begin{aligned}\dot{C}_1 &= v_1 - v_5 C_1 C_2 \\ \dot{C}_2 &= v_4 Y_2 - v_5 C_1 C_2 \\ \dot{Y}_1 &= v_2 C_1 - v_6 Y_1 \\ \dot{Y}_2 &= v_3 Y_1 - v_7 Y_2 \\ \dot{S} &= v_3 Y_1 - v_7 S\end{aligned}$$

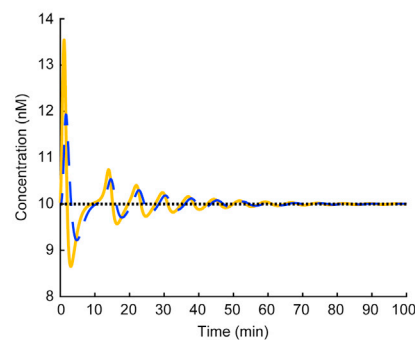
C



D



E



— Derivative of the input signal dU/dt
— Output signal X
⋯ Zero-level

Figure 3. Sensing the rate-of-change of the output of a synthetic regulatory biomolecular network through a Biomolecular Signal Differentiator

(A) Schematic of CRN (18) (network of interest) accompanied by a BioSD device (differentiator) which measures the speed of the output, Y_2 of the network via the sensing mechanism in Equation (20). We adopt the same arrow notation as in Figure 1 while the symbol ($:$) represents any of the three BioSD devices.

(B) ODE model capturing the dynamics of the topology given by Equations (18) and (20). As anticipated, the behavior of species Y_2 and S is described by the same equation.

(C) Input U of the differentiator coincides with species S and results from the simulation of the ODE model depicted in (B) with the following parameters: $v_1 = 2 \text{ nM min}^{-1}$, $v_2 = v_4 = 2 \text{ min}^{-1}$, $v_3 = 4 \text{ min}^{-1}$, $v_5 = 12 \text{ nM}^{-1} \text{ min}^{-1}$, $v_6 = v_7 = 1 \text{ min}^{-1}$.

(D) Simulation of BioSD-I (Equations (4a) and (4b)) response to the input shown in (C) using the following parameters: $k_{in} = 100 \text{ min}^{-1}$, $k_3 = b = 100 \text{ nM min}^{-1}$, $k_1 = 1 \text{ nM}^{-1} \text{ min}^{-1}$, $k_2 = 1 \text{ min}^{-1}$, $\delta = 0.5 \text{ min}^{-1}$. Equation (9) therefore yields $\epsilon = 0.01$. As can be seen, the output, X , of the differentiator is an accurate replica of the derivative of input U .

(E) The simulation in (D) is repeated after replacing the value of both k_{in} and k_3 with 10. Equation (9) therefore yields $\epsilon = 10$. Although the output, X , of the differentiator remains close to the derivative of input U , there is some loss of accuracy compared to (D). The respective simulations regarding BioSD-II and BioSD-III are presented in Figure S1. As expected, their responses are identical to those of BioSD-I.

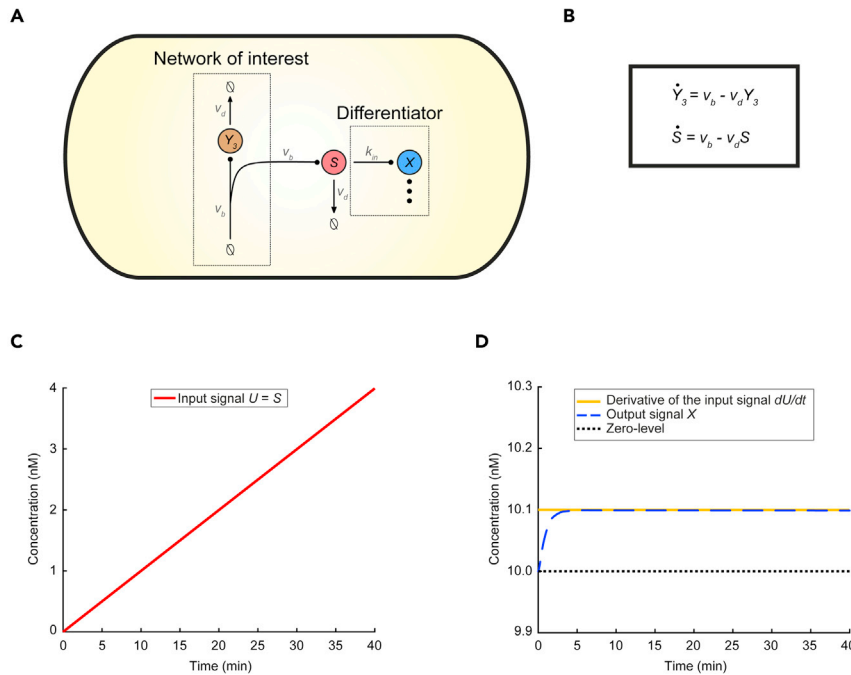


Figure 4. Sensing the rate-of-change of a production - removal biomolecular process through a Biomolecular Signal Differentiator

(A) Schematic of CRN (21) (network of interest) accompanied by a BioSD device (differentiator), which measures the speed of the output of the network (Y_3) via the sensing mechanism in Equation (20). We adopt the same arrow notation as in Figure 1 while the symbol (\emptyset) represents any of the three BioSD devices.

(B) ODE model capturing the dynamics of the topology given by Equations (20) and (21). As anticipated, the behavior of species Y_3 and S is described by the same equation.

(C) Input U of the differentiator coincides with species S and results from the simulation of the ODE model depicted in B with the following parameter values: $v_b = 0.1 \text{ nM min}^{-1}$, $v_d = 0.001 \text{ min}^{-1}$.

(D) Simulation of the BioSD-I (Equation (4a),(4b)) response to the input presented in (C) using the following parameters: $k_{in} = 10 \text{ min}^{-1}$, $k_3 = 10 \text{ nM min}^{-1}$, $b = 100 \text{ nM min}^{-1}$, $k_1 = 1 \text{ nM}^{-1} \text{ min}^{-1}$, $k_2 = 1 \text{ min}^{-1}$, $\delta = 0.5 \text{ min}^{-1}$ (same as in Figure 3E, $\epsilon = 10$). The output, X , of the differentiator is now an accurate replica of the derivative of input U . The latter (shown in C) belongs to the class of signals defined by Equations (7) and (17). The respective simulations regarding BioSD-II and BioSD-III are presented in Figure S2. As expected, their responses are identical to those of BioSD-I.

demonstrate that, for a given input signal, there exist sufficiently large values of ϵ for which the BioSD performance may not be satisfactory due to some loss of accuracy (discussed in Achieving biological signal differentiation).

We now replace the circuit described by (18) with the general production-removal process:



maintaining the same type of interconnection, as illustrated in Figure 4. Although the response of this process eventually converges to an equilibrium, for some period of time it practically increases linearly with time. Here, we focus on this linear regime of the response which is clearly aligned with Equation (17). Thus, as can be seen from Figure 4, BioSD networks are now able to provide accurate signal differentiation regardless of the high value of ϵ which, in the case of Figure 3, lead to a noticeable loss of accuracy.

Response to input signals corrupted by high-frequency noise

Potentially the most important problem of differentiator devices is their sensitivity to high-frequency noise components which the applied input signal may contain (Åström and Murray, 2021). To this end, we consider an input signal with a time-varying component

$$U^{TV} = \underbrace{A_u \sin(\omega_u t + \varphi_u)}_{\text{useful information}} + \underbrace{A_d \sin(\omega_d t + \varphi_d)}_{\text{noise}} \quad (\text{Equation 22})$$

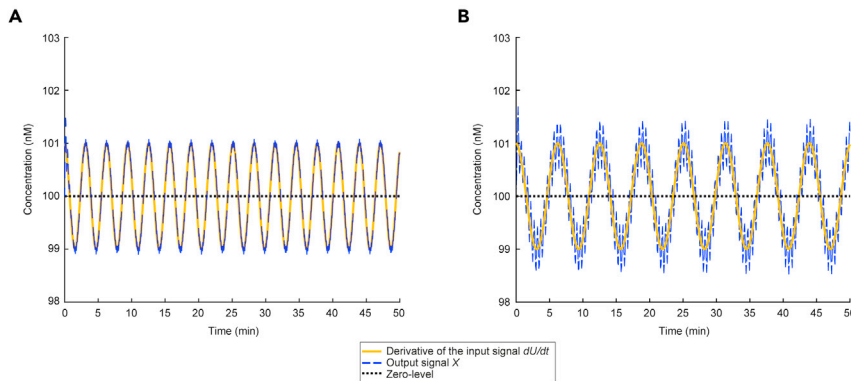


Figure 5. Response of Biomolecular Signal Differentiators to input signals with undesired high frequency components

(A) Without loss of generality we select BioSD-I (Equations (4a) and (4b)) to plot: A simulated response to an input of the form given by Equations (7) and (22) using the following parameters: $U^* = 1.2$ nM, $A_u = 1$ nM, $\omega_u = 1$ rad min⁻¹, $A_d = 0.2$ nM, $\omega_d = 400$ rad min⁻¹, $\varphi_u = \varphi_d = 0$ rad, $k_m = 100$ min⁻¹, $k_3 = b = 100$ nM min⁻¹, $k_1 = 1$ nM⁻¹ min⁻¹, $k_2 = 1$ min⁻¹, $\delta = 0.5$ min⁻¹. Equation (9) therefore yields $\epsilon = 0.0484$. Consequently, with respect to the input signal, the frequency of the undesired component (noise) is 400 times higher than that of the component of interest (useful information). It is evident that significant noise attenuation takes place and the accuracy of signal differentiation therefore remains very high.

(B) The simulation in (A) is repeated after changing the value of ω_d to 50 which makes the noise 50 times faster compared to the useful information. As can be seen, there is a decrease in the accuracy level of signal differentiation since the input noise of this frequency cannot be filtered adequately. For demonstration purposes, in both (A) and (B) we have chosen a baseline (around of which derivative action is carried out) much larger than the amplitudes of the (ideal) derivatives regarding all the input stimuli. The useful information is represented by a signal component whose (ideal) derivative has an amplitude much smaller than the one of the (ideal) derivative of the noise. Consequently, the former can be drowned out by the latter if no noise attenuation is performed.

where the actual signal we want to differentiate—useful information—is accompanied by undesired fluctuations (noise) arising, for instance, from unintended cross-talk interactions (Del Vecchio and Murray, 2015). Note that although we model both the useful information and the noise as sinusoids, this is without loss of generality as they can be thought of as Fourier components of more general signals (see STAR Methods Signals under consideration). Assuming perfect differentiation, we get:

$$\dot{U}^{TV} = \underbrace{\omega_u A_u \sin\left(\omega_u t + \varphi_u + \frac{\pi}{2}\right)}_{\text{derivative of useful information}} + \underbrace{\omega_d A_d \sin\left(\omega_d t + \varphi_d + \frac{\pi}{2}\right)}_{\text{derivative of noise}} \quad (\text{Equation 23})$$

Hence, even if the level of input corruption is low (e.g., A_d is much smaller than A_u - Equation (22)), the damage in the output of a perfect differentiator may be detrimental in case of a rapidly fluctuating noise signal (ω_d high). That is, $\omega_d A_d$ can be made arbitrarily large compared to $\omega_u A_u$ (Equation (23)) and, therefore, it is possible for the derivative of the useful signal to be completely drowned out by the derivative of some high frequency input noise. It is also apparent that the behavior of such an ideal differentiator module in the cellular environment is undesirable since it can lead to generation of greatly amplified output signals, which can be catastrophic.

Interestingly, the BioSD topologies allow us to deal with this noise amplification by suitably adjusting ϵ . As already discussed, BioSDs possess a low-pass filtering property defined by ϵ (see Equation (10)). Although this may be viewed as an “imperfection” in terms of their signal differentiation ability, it turns out to be a saving feature of great significance. Recalling the performance metric given by Equation (10) which coincides with the frequency response of the embedded filter and the Bode plot of Figure 2, we can see that there is a range of high frequencies over which signal attenuation can be effectively performed (see also STAR Methods Behavior analysis of biomolecular signal differentiators and Figure S3). This implies that Equation (15) approaches zero. Moreover, as ϵ increases, this range expands toward lower frequencies. Nevertheless, between the aforementioned range and the low-frequency one corresponding to signal differentiation, we can detect the existence of a relatively narrow frequency band where BioSD circuits may not be able to differentiate or attenuate input signals with satisfactory accuracy. The characteristics described above are demonstrated in Figure 5.

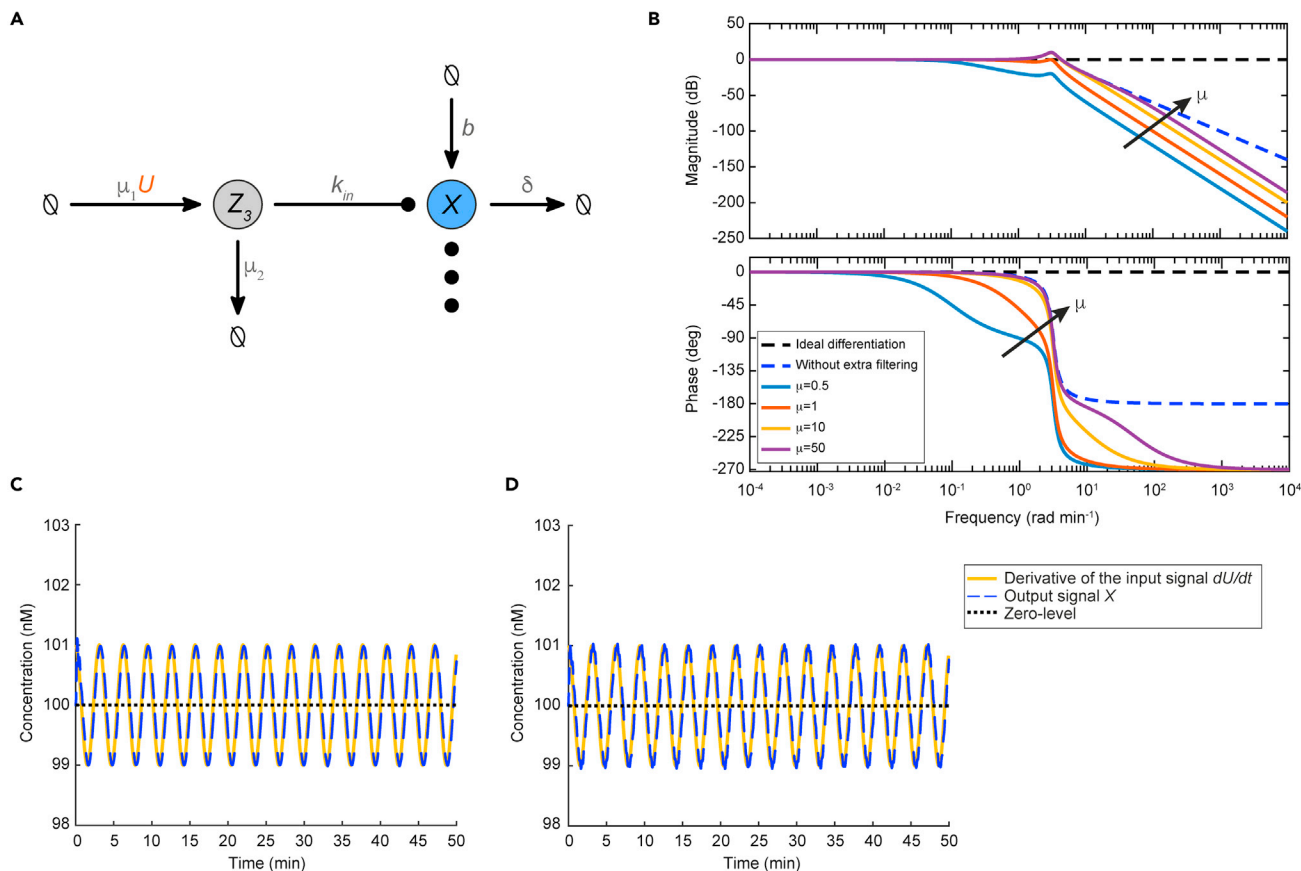


Figure 6. An alternative version of Biomolecular Signal Differentiators with an enhanced capability of input noise filtering

(A) Schematic structure of BioSD^F. We adopt the same arrow notation as in Figure 1 while the symbol (:) represents the remaining reactions composing any of the three BioSD devices. (B) Bode plot of the performance metric given by Equation (25) with $\epsilon = 0.1$. We consider different values of μ , where $\mu = \mu_1 = \mu_2$, that correspond to solid lines of different colors while the increasing direction of μ indicated by an arrow. We also depict the bode plot (magnitude and phase) of Equation (14) for the same value of ϵ and the case of ideal differentiation which are represented by blue and black dashed lines, respectively. In addition, for comparison purposes, we focus on a BioSD^F device based on BioSD-I to re-plot the simulation of c Figures 5A and d Figure 5B for the same values of the mutual parameters and $\mu_1 = \mu_2 = 5 \text{ min}^{-1}$. It is apparent that in both (C) and (D) very strong input noise attenuation takes place and the differentiation of the useful signal is thus conducted with significantly high accuracy.

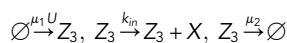
A structural addition for enhanced performance

In case there are increased requirements for noise reduction that cannot be easily met via parameter tuning, we present an alternative version of the BioSD networks with higher noise insensitivity, which we call BioSD^F (Figure 6A). These topologies are described by the same CRNs presented in the section Biological structure, but amended appropriately.

More analytically, recalling the CRNs given by Equations (1), (2), and (3), we see that input signals are applied to BioSD modules through the reaction:



In BioSD^F topologies, the above is replaced by the following set of reactions:



The additional species Z_3 is produced by the input species and degrades in the traditional manner while it catalyzes the formation of the output species. This structural addition is inspired by the work in (Samoilov et al., 2002; Laurenti et al., 2018), where biomolecular concepts from the area of signal processing were studied. In the following, we briefly present the main features of BioSD^F modules – a comprehensive

analysis of their behavior can be found in [STAR Methods An alternative version of biomolecular signal differentiators](#) (Figures S4 and S5).

The input/output relation of BioSD^F networks in the Laplace domain can be described by the transfer function:

$$\tilde{\Delta}_{\text{BioSD}^F}(s) = \frac{\mu_1}{s + \mu_2} \cdot \frac{s}{\varepsilon(s^2 + s) + 1} \quad (\text{Equation 24})$$

Similarly to BioSDs, we introduce the (normalized) performance metric:

$$\tilde{\Lambda}_F(j\omega) = \frac{\mu_2 \tilde{X}_{nF}(j\omega)}{\mu_1 \tilde{X}_{nd}(j\omega)} = \frac{\mu_2}{j\omega + \mu_2} \frac{1}{\varepsilon(-\omega^2 + j\omega) + 1} \quad (\text{Equation 25})$$

where $\tilde{X}_{nF}(j\omega)$ refers to the output of a BioSD^F network.

Using the magnitude-phase representation of [Equation \(25\)](#) we get:

$$|\tilde{\Lambda}_F(j\omega)| = \frac{1}{\sqrt{1 + \left(\frac{\omega}{\mu_2}\right)^2}} \frac{1}{\sqrt{\varepsilon^2\omega^2 + (1 - \varepsilon\omega^2)^2}} \quad (\text{Equation 26})$$

and

$$\angle \tilde{\Lambda}_F(j\omega) = \arctan\left(\frac{-\varepsilon\omega}{1 - \varepsilon\omega^2}\right) + \arctan\left(\frac{-\omega}{\mu_2}\right)$$

When $\tilde{\Lambda}_F(j\omega)$ is close to $1 \angle 0^\circ$ signal differentiation of high accuracy is achieved ([Figure 6B](#)) and the BioSD^F output can be approximated by:

$$X = \frac{\mu_1 k_{in}}{\mu_2 k_1 k_3} U + \frac{k_3}{k_2} \quad (\text{Equation 27})$$

Compared to the original BioSD topologies ([Equation \(16\)](#)), we now have two additional tuning parameters (μ_1, μ_2) with respect to the output differentiation gain when it comes to the low-frequency regime. However, the major advantage of this version of differentiators is an enhanced capability of noise filtering. In fact, we can have a greatly extended frequency range across which very strong attenuation of high frequency input noise can be achieved ([Figures 6C and 6D](#)). In that case, [Equation \(26\)](#) approaches zero. At the same time, the width of this frequency band depends on μ_2 and can be adjusted appropriately. As [Equation \(24\)](#) immediately reveals, the latter advantage stems from the fact that compared to BioSD circuits, BioSDs^F are equipped with an additional low-pass filter.

Biomolecular signal differentiators in natural regulatory networks

As outlined in the introduction, derivative action appears to be an important mechanism in various biological systems. To explore the biological relevance of the proposed BioSDs for cellular adaptations to environmental changes, we identified two naturally occurring and well-investigated regulatory network motifs that resemble the BioSD-II network. Note that these natural topologies are operating in the larger context of complex regulatory networks involving a plethora of signaling factors, some of which remain to be identified. We therefore describe the relevant motifs but do not comprehensively detail all interactions occurring in the biological system.

Stationary phase and starvation response - RpoS regulatory network

As shown in [Figure 7A](#), we found the BioSD-II motif in the context of adaptation to nutrient starvation and entry into stationary phase, which is mediated by the sigma factor RpoS in *E. coli* and related bacteria (reviewed in ([Battesti et al., 2011](#); [Hengge-Aronis, 2002](#))). Stress conditions, such as nutrient depletion or high pH, serve as the input U . While RpoS is present at low levels (b) in exponentially growing cells, its expression is substantially increased through both transcriptional and post-transcriptional regulation in response to environmental stresses or starvation ([Battesti et al., 2011](#)). One of the genes whose expression is dependent on RpoS is *rssB*, which encodes a response regulator. RssB binds to RpoS and mediates its degradation by the ClpXP protease ([Pruteanu and Hengge-Aronis, 2002](#)), thus functioning as Z_1 . Nutrient starvation also induces the expression of several anti-adaptor proteins (*Ira*; inhibitor of RssB activity). These proteins

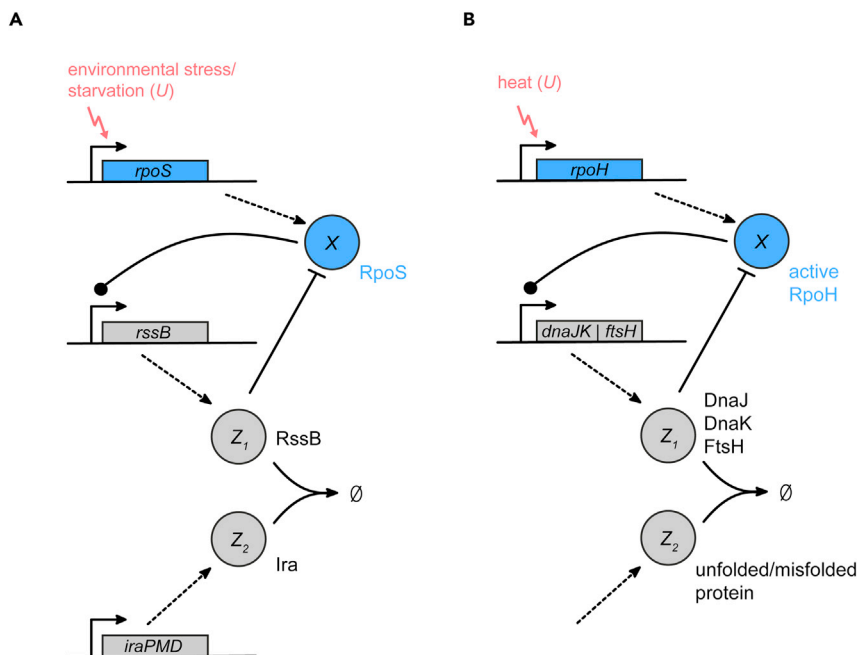


Figure 7. Examples of the Biomolecular Signal Differentiator-II motif in natural systems

Simplified schematics of BioSD-II topologies occurring as part of (A) the RpoS-mediated stress response and (B) the RpoH-mediated heat shock response in *Escherichia coli*. Corresponding components of BioSD-II are indicated.

bind to RssB and prevent RpoS degradation (Battesti et al., 2013), which corresponds to the action of Z_2 in BioSD-II.

Heat shock response - RpoH regulatory network

A second example for the BioSD-II motif was identified in the regulatory network of the sigma factor RpoH, which coordinates the heat shock response in *E. coli* (Figure 7B) (Straus et al., 1987; Roncarati and Scarlato, 2017). Upon heat shock, cellular RpoH levels rise above their low baseline concentration (b), inducing the expression of several chaperones (e.g. DnaKJ and GroELS) and proteases (e.g. FtsH and Lon). DnaK and DnaJ can bind to RpoH and facilitate its degradation by FtsH (Straus, Walter, and Gross, 1989a; Gamer et al., 1992), thereby acting as Z_1 . Unfolded or misfolded proteins will sequester chaperones and proteases (Gamer et al., 1992), thus increasing the stability of RpoH and fulfilling the function of Z_2 . In this network, the amount of active RpoH (as opposed to the total amount of RpoH) should be considered as X , since it has been found that the activity rather than the concentration of RpoH inside the cell drops during temperature downshifts (Straus, Walter, and Gross, 1989b).

Guidelines for experimental implementation of biomolecular signal differentiators

In addition to the natural regulatory networks described in the preceding section, here we outline possible synthetic implementations for all BioSD circuits inside a living cell and, in particular, in *E. coli* (Figure 8). Inducible expression of species X can be achieved from any well-characterized promoter, such as the IPTG-inducible P_{lac} . Leakiness of the lac promoter will ensure nonzero expression levels (b) even in the absence of inducer. Alternatively, if higher baseline expression levels are required, X could additionally be expressed from a weak constitutive promoter. To minimize undesirable interference with other cellular processes, X should be an orthogonal sigma factor, such as σ^F from *Bacillus subtilis* (Bervoets et al., 2018). A translational fusion of X to GFP will allow for easy tracking of the system output. σ^F will then induce expression of a Lon protease (Z in BioSD-I, Z_1 in BioSD-II and III) from its cognate promoter P_{F1} . In this case, a Lon⁻ strain of *E. coli* would be used to avoid interference of naturally present Lon protease. Addition of a degradation tag to σ^F will target it for degradation by the Lon protease. To approximate 0th-order degradation of Z in BioSD-I, an *ssrA* tag will be fused to the Lon protease as described in (Wong et al., 2007; Ang et al., 2010).

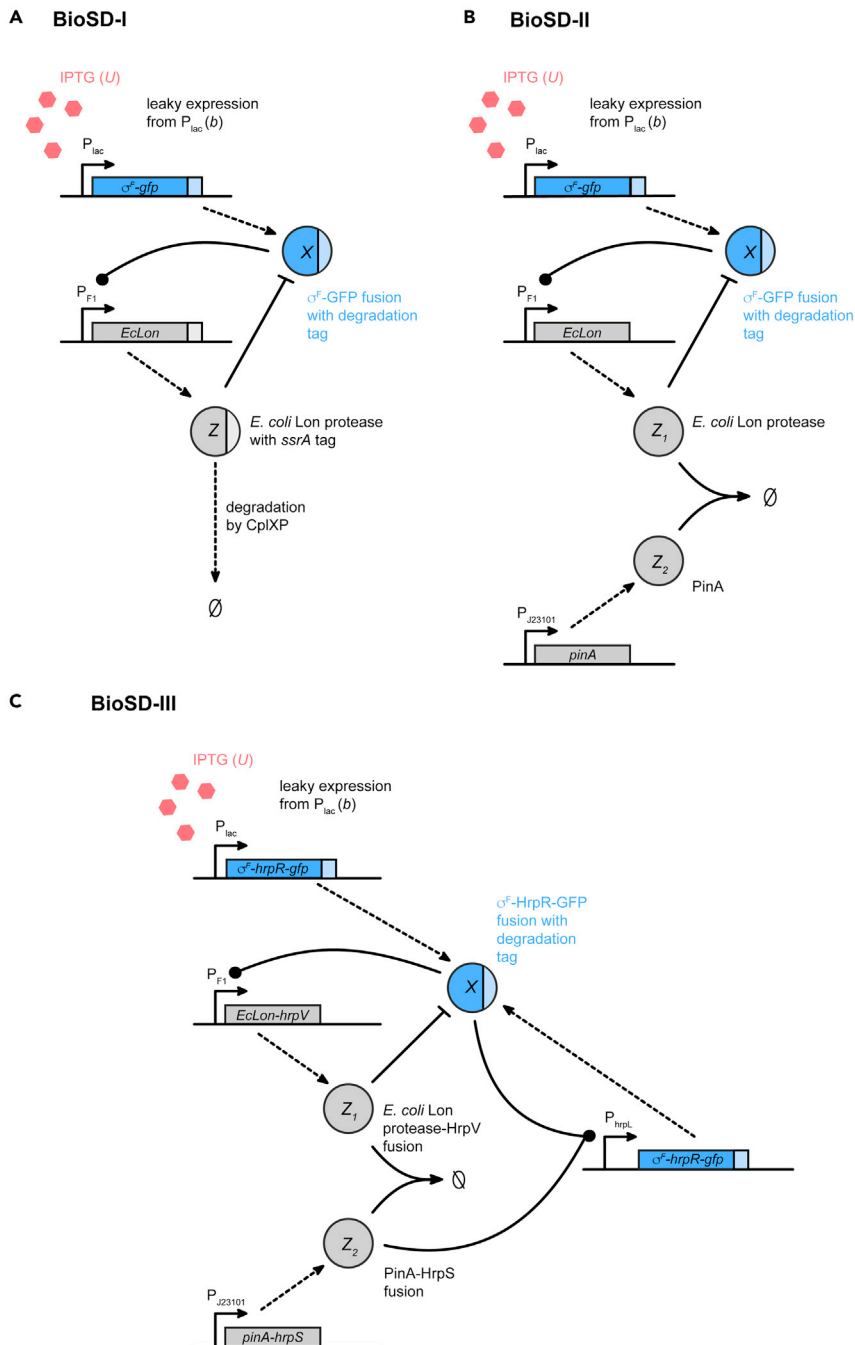


Figure 8. Possible experimental implementations of Biomolecular Signal Differentiators
Schematic representation of synthetic designs for ABioSD-I, BBioSD-II and CBioSD-III.

For BioSD-II, we additionally introduce constitutive expression of the protease inhibitor PinA from phage T4 (Z_2), which has been shown to specifically inhibit the Lon protease in *E. coli* with high affinity (Hilliard et al., 1998). A synthetic promoter from the BioBrick collection (Kelly et al., 2009) may be used to achieve the desired expression level of Z_2 . Ideally, an orthogonal Lon protease should be used (e.g. Lon protease from *Mesoplasma florum* (Aoki et al., 2019)) to prevent cross-talk with other cellular proteins. However, since the interaction of PinA with proteases has been characterized only in *E. coli* so far, we have suggested use of the *E. coli* Lon protease.

Due to the number of required interactions in BioSD-III, it will likely be necessary to introduce auxiliary species for X , Z_1 and Z_2 , which we refer to as X_{aux} , $Z_{1,aux}$ and $Z_{2,aux}$, respectively. These auxiliary species would ideally have identical behavior to the main species X , Z_1 and Z_2 , even though simulations indicate that completely identical behavior is not required (see [STAR Methods Analysis of the experimental topology of Biomolecular Signal Differentiator-III](#) and [Figure S6](#)). One option is to augment the design for BioSD-II with the Hrp system from *Pseudomonas syringae*, which has previously been implemented in synthetic biology studies ([Wang et al., 2014](#)). HrpR (X_{aux}) is expressed from P_{lac} together with σ^F , and HrpS ($Z_{2,aux}$) is expressed as a protein fusion with PinA. HrpR and HrpS are both required to induce additional production of σ^F and HrpR from P_{hrpL} . At the same time, HrpV ($Z_{1,aux}$) binds HrpS rendering it inactive. The structural addition required for BioSD^F can be implemented by, for example, expressing X from a T7 promoter and expressing T7 RNA polymerase (Z_3) from a separate inducible promoter.

DISCUSSION

In this study, we propose three biomolecular topologies that are able to act as highly accurate signal differentiators inside the cell. These designs provide guidance for building cellular devices capable of computing time derivatives of molecular signals. At the same time, they reveal concepts that are found in natural biological networks implementing differentiation and derivative feedback.

More specifically, we introduce three general biomolecular architectures BioSD-I, II, and III. Their generality lies in the fact that they are represented by CRNs without being restricted by the biological identity of reactants and products and, by extension, the corresponding biological pathway. Important structural components of the BioSDs are a negative feedback loop created by a special process of excitation and inhibition between two species ([Iglesias and Shi, 2014](#)), an enzymatic degradation of zero-order kinetics (BioSD-I), an autocatalytic-like reaction (BioSD-III) and an antithetic-like motif based on annihilation ([Oishi and Klavins, 2011](#); [Briat et al., 2016](#)) (BioSD-II, BioSD-III). We theoretically analyze their features and show the conditions under which high performance can be guaranteed. Among others, important concepts such as stability, tunability, and accuracy are discussed in detail.

Special emphasis is placed on the expected sensitivity of differentiators to input signals corrupted by high-frequency noise. We demonstrate that this issue can be resolved to a certain extent through suitable parameter tuning. Nevertheless, for cases in which stronger noise attenuation is needed, we present a structural modification that gives rise to three slightly different architectures, namely BioSD^F-I, II and III, with enhanced capabilities. However, the price for this improvement is the addition of an extra biomolecular species, which implies an increase in structural complexity. Moreover, we introduce performance metrics both for BioSDs and BioSDs^F based on which the circuit designer can assess the quality of signal differentiation and attenuation. These metrics take into account both the frequency content of the input signal and the reaction rates involved in the circuits, thus facilitating tuning according to the expected performance standards.

The ability to perform time differentiation is of central importance in various biological systems, contributing to stability and fast adaptation to changing conditions ([Barkai and Leibler, 1997](#); [Bazellières et al., 2015](#); [Cloutier and Wellstead, 2010](#)). Owing to the generality of the presented topologies, we anticipate that the present study will facilitate the investigation of naturally occurring systems capable of derivative action. In this study, we discuss the regulatory networks of two bacterial sigma factors, RpoS and RpoH, which play a central role in the response and adaptation to stress conditions and heat shock, respectively. Interestingly, these networks share structural characteristics with one of the proposed topologies, BioSD-II.

In addition, the motifs presented here provide building blocks that can be both implemented in stand-alone applications, such as speed biosensors, and also combined with existing biochemical control structures in a modular fashion, e.g., for building biomolecular PID controllers ([Chevalier et al., 2019](#)). We describe potential designs for synthetic experimental implementation of all three BioSDs, which can be readily adapted depending on the nature of the system and available biological parts. To realize the antithetic motif in BioSD-II and III, we propose the use of a protease/protease inhibitor pair as an alternative to the previously described systems using sigma and anti-sigma factors ([Aoki et al., 2019](#)) or sRNAs and mRNAs ([Huang et al., 2018](#); [Kelly et al., 2018](#)). To allow for greater flexibility in choosing the biomolecular species, we introduce a concept of auxiliary species whose usefulness is demonstrated through BioSD-III. Furthermore, to enhance the biological significance of our work in [STAR Methods Modeling a more realistic](#)

case of Biomolecular Signal Differentiator-II (Figures S7 and S8, Table S1), we investigate the behavior of one of the differentiator modules, namely BioSD-II, under more realistic conditions stemming from our experimental designs.

Stochasticity is an essential characteristic of biomolecular systems which operate in a noisy environment (Del Vecchio and Murray, 2015; Laurenti et al., 2018; Raj and Van Oudenaarden, 2008; Eldar and Elowitz, 2010; Cardelli et al., 2016; Warne et al., 2019). The biomolecular motifs introduced in the current study were analyzed through ODE models (deterministic analysis) which generally approximate well the dynamics of CRNs whose species are present in high copy-numbers. It therefore remains an interesting endeavor to identify the probabilistic effects of the molecular reactions involved that may have a significant impact on the behavior of these motifs when the biomolecular counts are low.

The speed or higher derivatives of the output of a system offers important information about its properties. For an electromechanical system this is not difficult, but it has been a challenging question for biological systems. In this article, we provide an approach to gain access to this information, which will be invaluable for assessing and improving the performance of biological systems. We believe that our BioSD topologies will expand the tools available for understanding and engineering biological systems for robustness and reliability.

Limitations of the study

As emphasized in the Discussion, the behavior of the topologies presented here is studied via deterministic mathematical analysis and simulations; the effect of inherent stochasticity of living systems stemming from the random nature of molecular reactions on these topologies is left for future work.

SUPPORTING CITATIONS

The following references appear in the supplemental information: Buchler and Louis, 2008; Fekkes et al., 1995; Gur et al., 2012; Schlosshauer and Baker, 2004.

STAR★METHODS

Detailed methods are provided in the online version of this paper and include the following:

- KEY RESOURCES TABLE
- RESOURCE AVAILABILITY
 - Lead contact
 - Materials availability
 - Data and code availability
- METHOD DETAILS
 - Signals under consideration
 - Equilibria and stability of biomolecular signal differentiators
 - The notion of strong rate of annihilation between Z_1 , Z_2 (large η) in Biomolecular Signal Differentiator-II
 - Behavior analysis of biomolecular signal differentiators
 - An alternative version of biomolecular signal differentiators
 - Analysis of the experimental topology of Biomolecular Signal Differentiator-III
 - Modeling a more realistic case of Biomolecular Signal Differentiator-II

SUPPLEMENTAL INFORMATION

Supplemental information can be found online at <https://doi.org/10.1016/j.isci.2021.103462>.

ACKNOWLEDGMENTS

This work was supported by funding from the Engineering and Physical Sciences Research Council (EPSRC) [grant numbers EP/M002454/1 and EP/L016494/1] and the Biotechnology and Biological Sciences Research Council (BBSRC) [grant number BB/M011224/1]. C.C.M.S. is supported by the Clarendon Fund (Oxford University Press) and the Keble College De Breyne Scholarship. L.C. is supported by a Royal Society Research Professorship.

AUTHOR CONTRIBUTIONS

Conceptualization and methodology, E.A., C.C.M.S., A.P., L.C.; Formal analysis and Software: E.A., Writing, E.A., C.C.M.S., A.P., L.C.; Supervision: A.P., L.C.

DECLARATION OF INTERESTS

The authors declare no competing interests.

Received: June 3, 2021

Revised: September 24, 2021

Accepted: November 12, 2021

Published: December 17, 2021

REFERENCES

- Alon, U. (2019). *An Introduction to Systems Biology: Design Principles of Biological Circuits* (CRC press).
- Ang, J., Bagh, S., Ingalls, B.P., and McMillen, D.R. (2010). Considerations for using integral feedback control to construct a perfectly adapting synthetic gene network. *J. Theor. Biol.* *266*, 723–738.
- Aoki, S.K., Lillacci, G., Gupta, A., Baumschlager, A., Schweingruber, D., and Khammash, M. (2019). A universal biomolecular integral feedback controller for robust perfect adaptation. *Nature* *570*, 533–537.
- Åström, K.J., and Murray, R.M. (2021). *Feedback Systems: An Introduction for Scientists and Engineers* (Princeton University Press).
- Baetica, A.A., Leong, Y.P., and Murray, R.M. (2020). Guidelines for designing the antithetic feedback motif. *Phys. Biol.* *17*, 055002.
- Barkai, N., and Leibler, S. (1997). Robustness in simple biochemical networks. *Nature* *387*, 913–917.
- Battesti, A., Hoskins, J.R., Tong, S., Milanesio, P., Mann, J.M., Kravats, A., Tsegaye, Y.M., Alexandre, B., Wickner, S., and Gottesman, S. (2013). Anti-adaptors provide multiple modes for regulation of the RssB adaptor protein. *Genes Develop.* *27*, 2722–2735.
- Battesti, Aurelia, NadimMajdalani, and Gottesman, S. (2011). The RpoS-mediated general stress response in *Escherichia coli*. *Annu. Rev. Microbiol.* *65*, 189–213.
- Bazellie'eres, E., Conte, V., Elosegui-Artola, A., Serra-Picamal, X., Bintanel-Morcillo, M., Roca-Cusachs, P., Muñoz, J.J., Sales-Pardo, M.a., Guimerà, R., and Trepat, X. (2015). Control of cell-cell forces and collective cell dynamics by the intercellular adhesome. *Nat. Cell Biol.* *17*, 409–420.
- Bervoets, I., Van Brempt, M., Van Nerom, K., Bob Van Hove, Maertens, J., De Mey, M., and Charlier, D.A. (2018). A sigma factor toolbox for orthogonal gene expression in *Escherichia coli*. *Nucleic Acids Res.* *46*, 2133–2144.
- Block, S.M., Segall, J.E., and Berg, H.C. (1983). Adaptation kinetics in bacterial chemotaxis. *J. Bacteriol.* *154*, 312–323.
- Briat, C., Gupta, A., and Khammash, M. (2016). Antithetic integral feedback ensures robust perfect adaptation in noisy biomolecular networks. *Cell Syst.* *2*, 15–26.
- Briat, C., Gupta, A., and Khammash, M. (2018). Antithetic proportional-integral feedback for reduced variance and improved control performance of stochastic reaction networks. *J. R. Soc. Interf.* *15*, 20180079.
- Buchler, N.E., and Louis, M. (2008). Molecular titration and ultrasensitivity in regulatory networks. *J. Mol. Biol.* *384*, 1106–1119.
- Cardelli, L., Kwiatkowska, M., and Laurenti, L. (2016). Stochastic analysis of chemical reaction networks using linear noise approximation. *Biosystems* *149*, 26–33.
- Chen, S., and Wilson, D.B. (1997). Construction and characterization of *Escherichia coli* genetically engineered for bioremediation of Hg²⁺-contaminated environments. *Appl. Environ. Microbiol.* *63*, 2442–2445.
- Chevalier, M., Gómez-Schiavon, M., Ng, A.H., and El-Samad, H. (2019). Design and analysis of a proportional-integral-derivative controller with biological molecules. *Cell Syst.* *9*, 338–353.
- Cloutier, M., and Wellstead, P. (2010). The control systems structures of energy metabolism. *J. R. Soc. Interf.* *7*, 651–665.
- Del Vecchio, D., Dy, A.J., and Qian, Y. (2016). Control theory meets synthetic biology. *J. R. Soc. Interf.* *13*, 20160380.
- Del Vecchio, D., and Murray, R.M. (2015). *Biomolecular Feedback Systems* (Princeton University Press).
- Del Vecchio, D., Ninfa, A.J., and Eduardo, D.S. (2008). Modular cell biology: retroactivity and insulation. *Mol. Syst. Biol.* *4*, 161.
- Eldar, A., and Elowitz, M.B. (2010). Functional roles for noise in genetic circuits. *Nature* *467*, 167–173.
- Fekkes, P.r., den Blaauwen, T., and Driessen, A.J.M. (1995). Diffusion-limited interaction between unfolded polypeptides and the *Escherichia coli* chaperone SecB. *Biochemistry* *34*, 10078–10085.
- Filo, M., and Khammash, M. (2021). A class of simple biomolecular antithetic proportional-integral-derivative controllers. *bioRxiv*. <https://doi.org/10.1101/2021.03.21.436342>.
- Gamer, J., Hermann, B., and Bukau, B. (1992). Physical interaction between heat shock proteins DnaK, DnaJ, and GrpE and the bacterial heat shock transcription factor σ^{32} . *Cell* *69*, 833–842.
- Gur, E., Vishkautzan, M., and Sauer, R.T. (2012). Protein unfolding and degradation by the AAA+ Lon protease. *Protein Sci.* *21*, 268–278.
- Halter, W., Murray, R.M., and Frank, A. (2019). Analysis of primitive genetic interactions for the design of a genetic signal differentiator. *Synth.Biol.* *4*, ysz015.
- Halter, W., Tuza, Z.A., and Frank, A. (2017). Signal differentiation with genetic networks. *IFAC-PapersOnLine* *50*, 10938–10943.
- Hancock, E.J., Jordan, A., Papachristodoulou, A., and Stan, G.B. (2017). The interplay between feedback and buffering in cellular homeostasis. *Cell Syst.* *5*, 498–508.
- Hengge-Aronis, R. (2002). Signal transduction and regulatory mechanisms involved in control of the σ S (RpoS) subunit of RNA polymerase. *Microbiol. Mol. Biol. Rev.* *66*, 373–395.
- Hilliard, J.J., Maurizi, M.R., and Lee, D.S. (1998). Isolation and characterization of the phage T4 PinA protein, an inhibitor of the ATP-dependent Lon protease of *Escherichia coli*. *J. Biol. Chem.* *273*, 518–523.
- Huang, H.H., Qian, Y., and Del Vecchio, D. (2018). A quasi-integral controller for adaptation of genetic modules to variable ribosome demand. *Nat. Commun.* *9*, 1–12.
- Iglesias, P.A., and Devreotes, P.N. (2008). Navigating through models of chemotaxis. *Curr.Opin.Cell Biol.* *20*, 35–40.
- Iglesias, P.A., and Shi, C. (2014). Comparison of adaptation motifs: temporal, stochastic and spatial responses. *IET Syst. Biol.* *8*, 268–281.
- Kelly, C.L., Harris, A.W.K., Harrison, S., Hancock, E.J., Heap, J.T., and Papachristodoulou, A. (2018). Synthetic negative feedback circuits using engineered small RNAs. *Nucleic Acids Res.* *46*, 9875–9889.
- Kelly, J.R., Rubin, A.J., Davis, J.H., Ajo-Franklin, C.M., Cumbers, J., Czar, M.J., de Mora, K.,

- Glieberman, A.L., Monie, D.D., and Drew, E. (2009). Measuring the activity of BioBrick promoters using an in vivo reference standard. *J. Biol. Eng.* 3, 1611–1754.
- Khalil, H.K. (2002). *Nonlinear Systems*, 3rd Ed. (Prentice-Hall, Inc).
- Lathi, B.P. (1998). *Signal Processing and Linear Systems* (Oxford University Press).
- Laurenti, L., Csikasz-Nagy, A., Kwiatkowska, M., and Cardelli, L. (2018). Molecular filters for noise reduction. *Biophys. J.* 114, 3000–3011.
- Lu, T.K., Khalil, A.S., and Collins, J.J. (2009). Next-generation synthetic gene networks. *Nat. Biotechnol.* 27, 1139.
- Macnab, R.M., and Koshland, D.E. (1972). The gradient-sensing mechanism in bacterial chemotaxis. *Proc. Natl. Acad. Sci.* 69, 2509–2512.
- Modi, S., Dey, S., and Singh, A. (2019). Proportional and derivative controllers for buffering noisy gene expression. In 2019 IEEE 58th Conference on Decision and Control (CDC) (IEEE), pp. 2832–2837.
- Oishi, K., and Klavins, E. (2011). Biomolecular implementation of linear I/O systems. *IET Syst. Biol.* 5, 252–260.
- Olsman, N.h., Baetica, A.A., Xiao, F., Leong, Y.P., Murray, R.M., and Doyle, J.C. (2019a). Hard limits and performance tradeoffs in a class of antithetic integral feedback networks. *Cell Syst.* 9, 49–63.
- Olsman, N., Xiao, F., and Doyle, J.C. (2019b). Architectural principles for characterizing the performance of antithetic integral feedback networks. *Iscience* 14, 277–291.
- Olsman, N., and Forni, F. (2020). Antithetic integral feedback for the robust control of monostable and oscillatory biomolecular circuits. *IFAC-PapersOnLine* 53, 16826–16833.
- Oppenheim, A.V., Willsky, A.S., and Hamid Nawab, S. (1996). *Signals Systems*, 2nd Ed. (Prentice-Hall, Inc).
- Paulino, N.M.G., Foo, M., Kim, J., and Bates, D.G. (2019). PID and state feedback controllers using DNA strand displacement reactions. *IEEE Control Syst. Lett.* 3, 805–810.
- Pieper, D.H., and Reineke, W. (2000). Engineering bacteria for bioremediation. *Curr.Opin.Biotechnol.* 11, 262–270.
- Pruteanu, M., and Hengge-Aronis, R. (2002). The cellular level of the recognition factor RssB is rate-limiting for σ S proteolysis: implications for RssB regulation and signal transduction in σ S turnover in *Escherichia coli*. *Mol. Microbiol.* 45, 1701–1713.
- Qian, Y., and Del Vecchio, D. (2018). Realizing ‘integral control’ in living cells: how to overcome leaky integration due to dilution? *J. R. Soc. Interf.* 15, 20170902.
- Raj, A., and Van Oudenaarden, A. (2008). Nature, nurture, or chance: stochastic gene expression and its consequences. *Cell* 135, 216–226.
- Roncarati, D., and Scarlato, V. (2017). Regulation of heat-shock genes in bacteria: from signal sensing to gene expression output. *FEMS Microbiol. Rev.* 41, 549–574.
- Samaniego, C.C., Giordano, G., and Franco, E. (2019). Practical differentiation using ultrasensitive molecular circuits. In 2019 18th European Control Conference (ECC) (IEEE), pp. 692–697.
- Samaniego, C.C., Kim, J., and Franco, E. (2020). Sequestration and delays enable the synthesis of a molecular derivative operator. In 2020 59th IEEE Conference on Decision and Control (CDC) (IEEE), pp. 5106–5112.
- Samoilov, M., Adam, A., and Ross, J. (2002). Signal processing by simple chemical systems. *J. Phys. Chem. A* 106, 10205–10221.
- Schlosshauer, M., and Baker, D. (2004). Realistic protein–protein association rates from a simple diffusional model neglecting long-range interactions, free energy barriers, and landscape ruggedness. *Protein Sci.* 13, 1660–1669.
- Shimizu, T.S., Tu, Y., and Berg, H.C. (2010). A modular gradient-sensing network for chemotaxis in *Escherichia coli* revealed by responses to time-varying stimuli. *Mol. Syst. Biol.* 6, 382.
- Steel, H., Lillacci, G., Khammash, M., and Papachristodoulou, A. (2017). Challenges at the interface of control engineering and synthetic biology. In 2017 IEEE 56th Annual Conference on Decision and Control (CDC) (IEEE), pp. 1014–1023.
- Straus, D.B., Walter, W.A., and Gross, C.A. (1987). The heat shock response of *E. coli* is regulated by changes in the concentration of σ 32. *Nature* 329, 348–351.
- Straus, D.B., Walter, W.A., and Gross, C.A. (1989a). DnaK, DnaJ, and GrpE heat shock proteins negatively regulate heat shock gene expression by controlling the synthesis and stability of σ 32. *Genes Develop.* 4, 2202–2209.
- Straus, D.B., A Walter, W., and Gross, C.A. (1989b). The activity of σ 32 is reduced under conditions of excess heat shock protein production in *Escherichia coli*. *Genes Development* 3, 2003–2010.
- Wang, B., Barahona, M., and Buck, M. (2014). Engineering modular and tunable genetic amplifiers for scaling transcriptional signals in cascaded gene networks. *Nucleic Acids Res.* 42, 9484–9492.
- Warne, D.J., Baker, R.E., and Simpson, M.J. (2019). Simulation and inference algorithms for stochastic biochemical reaction networks: from basic concepts to state-of-the-art. *J. R. Soc. Interf.* 16, 20180943.
- Whitby, M., Cardelli, L., Kwiatkowska, M., Laurenti, L., Tribastone, M., and Tschaikowski, M. (2021). PID control of biochemical reaction networks. *IEEE Trans. Automat.Control* 7, 1.
- Wilson, H.R. (1999). *Spikes, Decisions, and Actions: The Dynamical Foundations of Neurosciences* (Oxford University Press).
- Wong, W.W., Tsai, T.Y., and Liao, J.C. (2007). Single-cell zeroth-order protein degradation enhances the robustness of synthetic oscillator. *Mol. Syst. Biol.* 3, 1–8.
- Zill, D.G. (2012). *A First Course in Differential Equations with Modeling Applications* (Cengage Learning).

STAR★METHODS

KEY RESOURCES TABLE

REAGENT or RESOURCE	SOURCE	IDENTIFIER
Software and algorithms		
MATLAB	Mathworks	www.mathworks.com
Matlab code used for simulations	This study	https://github.com/emgalox/BioS-Differentiators

RESOURCE AVAILABILITY

Lead contact

Further information and requests for resources and reagents should be directed to and will be fulfilled by the lead contact, Antonis Papachristodoulou (antonis@eng.ox.ac.uk).

Materials availability

This study did not generate new unique materials.

Data and code availability

All numerical simulations were performed in MATLAB R2020 using the ODE solver ode23s except for those in Figure 5 where the ODE solver ode113 was used. Simulation parameter values can be found in the figure captions. Initial conditions for the biomolecular species involved are considered zero except for BioSDs and BioSDs^F where the corresponding equilibria ("rest-positions") are used (see STAR Methods Equilibria and stability of Biomolecular Signal Differentiators and An alternative version of Biomolecular Signal Differentiators). The corresponding programming code is available at: <https://github.com/emgalox/BioS-Differentiators>.

METHOD DETAILS

Signals under consideration

In this study we consider Fourier-transformable signals (unless otherwise stated) (Lathi, 1998; Oppenheim et al., 1996). The Fourier transform exists for any signal, $s(t)$, satisfying the following conditions, also known as Dirichlet conditions:

- $s(t)$ is absolutely integrable, i.e.:

$$\int_{-\infty}^{+\infty} |s(t)| dt < \infty$$

- $s(t)$ has a finite number of maxima and minima within any finite interval.
- $s(t)$ has a finite number of discontinuities within any finite interval. In addition, each of these discontinuities must be finite.

The Dirichlet conditions are sufficient but not necessary for the existence of Fourier transform of a signal. Moreover, it should be noted that the Fourier transform of periodic signals can be computed from their Fourier series representation (assuming it exists) with the help of impulse functions.

The main idea behind Fourier analysis is the decomposition of a signal into a sum of sinusoids, the relative amplitudes and phases of which are determined by the Fourier spectrum of that signal. In the case of a linear, time invariant system, transmission of a signal can be therefore treated as transmission of its constituent sinusoids. Moreover, the frequency-domain description of such a system using its frequency response is an alternative to the time-domain description based on convolution.

Finally, in the current study we focus on physical signals that can be generated in a cellular environment. Such naturally-occurring signals typically satisfy the Dirichlet conditions and, thus, have a Fourier representation - signals that do not satisfy these conditions do not normally arise in practical applications. Further details on the above can be found in (Lathi, 1998; Oppenheim et al., 1996).

Equilibria and stability of biomolecular signal differentiators

We assume that all biomolecular circuits in this study are represented by chemical reaction networks (CRNs) whose dynamics are described by the law of mass action unless otherwise stated. For the purposes of deterministic modeling, we consider inputs $U(t)$ that are bounded, non-negative, continuous-time signals of finite duration, the time derivatives of which exist and are also bounded and continuous. This is clearly aligned with the biological nature of $U(t)$ which can correspond, for example, to the concentration of a biomolecular species.

Biomolecular signal differentiator-I. Biomolecular Signal Differentiator-I (BioSD-I) is described by the CRN:



where $k_{in}, b, k_2, k_1, k_3, \delta \in \mathbb{R}_+$. Note that the removal rate of Z is constant and equal to k_3 . To achieve this we assume that Z participates in an enzyme-catalyzed degradation process which is traditionally described by Michaelis-Menten kinetics. More precisely, the removal rate of Z is equal to

$$k_3 \frac{Z}{Z + K_m} \quad (\text{Equation S2})$$

where $K_m \in \mathbb{R}_+$ is the Michaelis-Menten constant. When the enzyme that catalyzes the degradation process is saturated by its substrate, we have:

$$Z \gg K_m \quad (\text{Equation S3})$$

which entails, in effect, zero-order kinetics since Equation (S2) becomes practically equal to k_3 .

The dynamics of the above CRN (Equation (S1)) are given by the following system of Ordinary Differential Equations (ODEs):

$$\dot{X} = k_{in}U + b - k_1XZ - \delta X \quad (\text{Equation S4})$$

$$\dot{Z} = k_2X - k_3 \quad (\text{Equation S5})$$

For any constant input U^* , a steady state (X^*, Z^*) of the system given by Equations (S4) and (S5) exists and is finite. By setting the time derivatives of this system to zero, we can obtain the following unique steady-state:

$$X^* = \frac{k_3}{k_2} \quad (\text{Equation S6})$$

$$Z^* = \frac{k_2(k_{in}U^* + b)}{k_1k_3} - \frac{\delta}{k_1} \quad (\text{Equation S7})$$

Clearly X^* is positive while, due to Equation (S3), the same is true for Z^* (in fact: $Z^* \gg 0$).

To study the local stability of the above equilibrium, we linearize Equations (S4) and (S5) around (X^*, Z^*) for a constant input U^* to get:

$$\begin{bmatrix} \dot{X} \\ \dot{Z} \end{bmatrix} = \underbrace{\begin{bmatrix} -\frac{k_2(k_{in}U^* + b)}{k_3} & -\frac{k_1k_3}{k_2} \\ k_2 & 0 \end{bmatrix}}_{G_1} \begin{bmatrix} X \\ Z \end{bmatrix} \quad (\text{Equation S8})$$

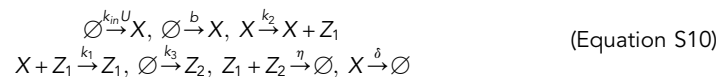
As far as the linear system described by Equation (S8) is concerned, the steady state (X^*, Z^*) is exponentially stable since matrix G_1 is Hurwitz. To prove this, we find the characteristic polynomial of G_1 as:

$$P_1(s) = \det(sI - G_1) = s^2 + \frac{k_2}{k_3}(k_{in}U^* + b)s + k_1k_3 \quad (\text{Equation S9})$$

According to Routh-Hurwitz criterion, the second-order polynomial given by Equation (S9) has both roots in the open left half plane if, and only if, both $\frac{k_2(k_{in}U^* + b)}{k_3}$ and k_1k_3 are positive, which is always true. Consequently, (X^*, Z^*) is a positive locally exponentially stable steady state for the nonlinear system given by Equations (S4) and (S5).

Following the same procedure, we next analyze BioSD-II and BioSD-III.

Biomolecular signal differentiator-II. The CRN that corresponds to Biomolecular Signal Differentiator-II (BioSD-II) is:



where $k_{in}, b, k_2, k_1, \delta, \eta \in \mathbb{R}_+$.

The dynamics of the above CRN (Equation (S10)) are described by the set of ODEs:

$$\dot{X} = k_{in}U + b - k_1XZ_1 - \delta X \quad (\text{Equation S11})$$

$$\dot{Z}_1 = k_2X - \eta Z_1Z_2 \quad (\text{Equation S12})$$

$$\dot{Z}_2 = k_3 - \eta Z_1Z_2 \quad (\text{Equation S13})$$

For any constant input U^* , provided that:

$$k_2(k_{in}U^* + b) > \delta k_3, \quad (\text{Equation S14})$$

we have a unique positive (finite) steady state:

$$X^* = \frac{k_3}{k_2} \quad (\text{Equation S15})$$

$$Z_1^* = \frac{k_2(k_{in}U^* + b)}{k_1k_3} - \frac{\delta}{k_1} \quad (\text{Equation S16})$$

$$Z_2^* = \frac{k_3}{\eta \left(\frac{k_2(k_{in}U^* + b)}{k_1k_3} - \frac{\delta}{k_1} \right)} \quad (\text{Equation S17})$$

We now linearize Equations (S11), (S12), and (S13) around the fixed point defined by Equations (S15), (S16), and (S17) to obtain:

$$\begin{bmatrix} \dot{X} \\ \dot{Z}_1 \\ \dot{Z}_2 \end{bmatrix} = \underbrace{\begin{bmatrix} -\frac{k_2(k_{in}U^* + b)}{k_3} & -\frac{k_1k_3}{k_2} & 0 \\ k_2 & -\eta Z_2^* & -\eta Z_1^* \\ 0 & -\eta Z_2^* & -\eta Z_1^* \end{bmatrix}}_{G_2} \begin{bmatrix} X \\ Z_1 \\ Z_2 \end{bmatrix}$$

The characteristic polynomial of G_2 is:

$$P_2(s) = \det(sI - G_2) = s^3 + \alpha_2s^2 + \alpha_1s + \alpha_0 \quad (\text{Equation S18})$$

where

$$\alpha_2 = \sigma + \eta(Z_1^* + Z_2^*) \quad (\text{Equation S19})$$

$$\alpha_1 = k_1k_3 + \sigma\eta(Z_1^* + Z_2^*) \quad (\text{Equation S20})$$

$$\alpha_0 = k_1k_3\eta Z_1^* \quad (\text{Equation S21})$$

and

$$\sigma = \frac{k_2(k_{in}U^* + b)}{k_3}$$

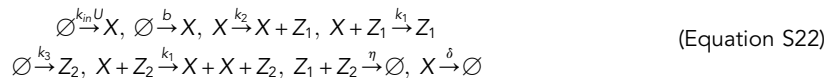
The polynomial given by Equation (S18) has all roots in the open-half plane if and only if α_2, α_0 are positive and $\alpha_2\alpha_1 > \alpha_0$ (Routh-Hurwitz criterion). Indeed:

$$\begin{aligned} &(\sigma + \eta(Z_1^* + Z_2^*)) (k_1 k_3 + \sigma \eta(Z_1^* + Z_2^*)) > \eta k_1 k_3 Z_1^* \\ \text{or} \\ &\sigma k_1 k_3 + \sigma^2 \eta(Z_1^* + Z_2^*) + k_1 k_3 \eta(Z_1^* + Z_2^*) + \sigma \eta^2 (Z_1^* + Z_2^*)^2 > \eta k_1 k_3 Z_1^* \\ \text{or} \\ &\sigma k_1 k_3 + \sigma^2 \eta(Z_1^* + Z_2^*) + \sigma \eta^2 (Z_1^* + Z_2^*)^2 + \eta k_1 k_3 Z_2^* > 0 \end{aligned}$$

which is always true since all the quantities involved are positive. Therefore, (X^*, Z_1^*, Z_2^*) is a positive locally exponentially stable steady state (G_2 is Hurwitz) for the nonlinear system described by Equations (S11), (S12), and (S13).

Note that outside the parameter regime defined by Equation (S14) BioSD-II is unable to reach equilibrium. In particular, assuming non-negative initial conditions for Equations (S11), (S12), and (S13) (which is always the case because the variables involved represent biomolecular concentrations) the states of the latter remain always non-negative (as expected from mass action kinetics). Indeed, when $X = 0$, Equation (S11) implies $\dot{X} = k_{in}U + b > 0$. Furthermore, when $Z_1 = 0$, Equation (S12) results in $\dot{Z}_1 = k_2 X \geq 0$ and, finally, when $Z_2 = 0$, Equation (S13) imposes $\dot{Z}_2 = k_3 > 0$. However, outside the parameter regime in question, one of the following must hold: $k_2(k_{in}U^* + b) < \delta k_3$ or $k_2(k_{in}U^* + b) = \delta k_3$. In the first scenario, it is apparent from Equations (S16) and (S17) that the steady state of Z_1, Z_2 becomes negative while in the second case Equation (S17) indicates that Z_2 tends to infinity - thus, BioSD-II cannot approach a finite steady state.

Biomolecular signal differentiator-III. Biomolecular Signal Differentiator-III (BioSD-III) is represented by the CRN:



where $k_{in}, b, k_2, k_1, \delta, \eta \in \mathbb{R}_+$.

The corresponding ODE model describing the dynamics is

$$\dot{X} = k_{in}U + b - k_1 X Z_1 + k_1 X Z_2 - \delta X \quad \text{(Equation S23)}$$

$$\dot{Z}_1 = k_2 X - \eta Z_1 Z_2 \quad \text{(Equation S24)}$$

$$\dot{Z}_2 = k_3 - \eta Z_1 Z_2 \quad \text{(Equation S25)}$$

For any constant input U^* , we have a unique positive steady state (providing that it exists and is finite):

$$X^* = \frac{k_3}{k_2} \quad \text{(Equation S26)}$$

$$Z_1^* = \frac{1}{2} \left[\frac{k_2(k_{in}U^* + b)}{k_1 k_3} - \frac{\delta}{k_1} \right] + \frac{1}{2} \sqrt{\left[\frac{k_2(k_{in}U^* + b)}{k_1 k_3} - \frac{\delta}{k_1} \right]^2 + 4 \frac{k_3}{n}} \quad \text{(Equation S27)}$$

$$Z_2^* = -\frac{1}{2} \left[\frac{k_2(k_{in}U^* + b)}{k_1 k_3} - \frac{\delta}{k_1} \right] + \frac{1}{2} \sqrt{\left[\frac{k_2(k_{in}U^* + b)}{k_1 k_3} - \frac{\delta}{k_1} \right]^2 + 4 \frac{k_3}{n}} \quad \text{(Equation S28)}$$

Linearizing the system given by Equations (S23), (S24), and (S25) around its steady state (Equations (S26), (S27), and (S28)) yields:

$$\begin{bmatrix} \dot{X} \\ \dot{Z}_1 \\ \dot{Z}_2 \end{bmatrix} = \underbrace{\begin{bmatrix} \frac{k_2(k_{in}U^* + b)}{k_3} & -\frac{k_1 k_3}{k_2} & \frac{k_1 k_3}{k_2} \\ k_2 & -\eta Z_2^* & -\eta Z_1^* \\ 0 & -\eta Z_2^* & -\eta Z_1^* \end{bmatrix}}_{G_3} \begin{bmatrix} X \\ Z_1 \\ Z_2 \end{bmatrix}$$

The characteristic polynomial of G_3 is:

$$P_3(s) = \det(sI - G_3) = s^3 + \alpha_2 s^2 + \alpha_1 s + \alpha_0 \quad \text{(Equation S29)}$$

where α_2, α_1 are identical to α_2 (Equation S19), α_1 (Equation S20), respectively and:

$$\alpha_0 = k_1 k_3 \eta (Z_1^* + Z_2^*)$$

In order to show that G_3 is Hurwitz we need to verify that $\alpha_2 \alpha_1 > \alpha_0$ (from Routh-Hurwitz criterion).

This inequality is satisfied because:

$$\begin{aligned} &(\sigma + \eta(Z_1^* + Z_2^*))(k_1 k_3 + \sigma \eta(Z_1^* + Z_2^*)) > \eta k_1 k_3 (Z_1^* + Z_2^*) \\ \text{or} \\ &\sigma k_1 k_3 + \sigma^2 \eta (Z_1^* + Z_2^*) + k_1 k_3 \eta (Z_1^* + Z_2^*) + \sigma \eta^2 (Z_1^* + Z_2^*)^2 > k_1 k_3 \eta (Z_1^* + Z_2^*) \\ \text{or} \\ &\sigma k_1 k_3 + \sigma^2 \eta (Z_1^* + Z_2^*) + \sigma \eta^2 (Z_1^* + Z_2^*)^2 > 0 \end{aligned}$$

which is always true as a sum of positive quantities. Hence, (U^*, X^*, Z_1^*, Z_2^*) is a positive locally exponentially stable steady state for the nonlinear system described by Equations (S23), (S24), and (S25).

The notion of strong rate of annihilation between Z_1, Z_2 (large η) in Biomolecular Signal Differentiator-II

This reaction describes a process where species Z_1, Z_2 bind to each other irreversibly to form a product which can be considered as biologically inactive. In other words, this product does not participate in any of the reactions in BioSD-II. Here we demonstrate that the steady state of Z_2 as well as its deviation from it is practically negligible if the formation rate, η , of the product in question is sufficiently high. At the same time, the effect of Z_2 on the dynamics of BioSD-II can be considered insignificant, too.

By adopting the coordinate transformations: $u = U - U^*, x = X - X^*, z_1 = Z_1 - Z_1^*, z_2 = Z_2 - Z_2^*$ which denote small perturbations around (U^*, X^*, Z_1^*, Z_2^*) , we obtain through linearization of Equations (S11), (S12), and (S13):

$$\begin{bmatrix} \dot{x} \\ \dot{z}_1 \\ \dot{z}_2 \end{bmatrix} = \begin{bmatrix} \frac{k_2(k_{in}U^* + b)}{k_3} & -\frac{k_1 k_3}{k_2} & 0 \\ k_2 & -\eta Z_2^* & -\eta Z_1^* \\ 0 & -\eta Z_2^* & -\eta Z_1^* \end{bmatrix} \begin{bmatrix} x \\ z_1 \\ z_2 \end{bmatrix} + \begin{bmatrix} k_{in} \\ 0 \\ 0 \end{bmatrix} u \quad (\text{Equation S30})$$

We now introduce the non-dimensional variables:

$$t_n = \beta_1 t \quad (\text{Equation S31})$$

$$x_n = \frac{1}{\beta_2} x \quad (\text{Equation S32})$$

$$z_{1n} = \frac{\beta_1}{\beta_2 k_2} z_1 \quad (\text{Equation S33})$$

$$z_{2n} = \frac{\beta_1}{\beta_2 k_2} z_2 \quad (\text{Equation S34})$$

$$u_n = \frac{k_{in}}{\beta_1 \beta_2} u \quad (\text{Equation S35})$$

where

$$\beta_1 = \frac{k_3}{\left(\frac{k_2(k_{in}U^* + b)}{k_1 k_3} - \frac{\delta}{k_1}\right)} \quad (\text{Equation S36})$$

and β_2 is an arbitrary scaling parameter that carries the same units as x_n . In addition, we introduce the non-dimensional parameters:

$$\lambda_1 = \frac{\beta_1^2}{\eta k_3} \quad (\text{Equation S37})$$

$$\lambda_2 = \frac{k_2(k_{in}U^* + b)}{\beta_1 k_3} \quad (\text{Equation S38})$$

$$\lambda_3 = \frac{k_1 k_3}{\beta_1 k_2} \quad (\text{Equation S39})$$

By substituting Equations (S31), (S32), (S33), (S34), (S35), (S36), (S37), (S38), and (S39) into the model given by Equation (S30), we obtain:

$$\begin{aligned}\dot{x}_n &= u_n - \lambda_2 x_n - \lambda_3 z_{1n} \\ \dot{z}_{1n} &= k_2 x_n - z_{1n} - \frac{1}{\lambda_1} z_{2n} \\ \dot{z}_{2n} &= -z_{1n} - \frac{1}{\lambda_1} z_{2n}\end{aligned}$$

or

$$\begin{aligned}\dot{x}_n &= u_n - \lambda_2 x_n - \lambda_3 z_{1n} \\ \lambda_1 \dot{z}_{1n} &= \lambda_1 x_n - \lambda_1 z_{1n} - z_{2n} \\ \lambda_1 \dot{z}_{2n} &= -\lambda_1 z_{1n} - z_{2n}\end{aligned}$$

We now introduce the linear transformation $g_n = z_{1n} - z_{2n}$ resulting in the following mathematically equivalent system:

$$\dot{x}_n = u_n - \lambda_2 x_n - \lambda_3 g_n - \lambda_3 z_{2n} \quad \text{(Equation S40)}$$

$$\dot{g}_n = x_n \quad \text{(Equation S41)}$$

$$\lambda_1 \dot{z}_{2n} = -\lambda_1 g_n - (1 + \lambda_1) z_{2n} \quad \text{(Equation S42)}$$

According to Equation (S37), $\lambda_1 \rightarrow 0$ as $\eta \rightarrow \infty$. This means that we can make λ_1 negligible by choosing a large value for η :

$$\eta \gg \frac{\beta_1^2}{k_3} \quad \text{(Equation S43)}$$

We now regard λ_1 as a singular perturbation parameter and use Theorem 11.1 in (H. K. Khalil, 2002). From Equations (S40), (S41), and (S42) we obtain the following reduced model for $\lambda_1 = 0$:

$$\dot{x}_n = u_n - \lambda_2 x_n - \lambda_3 g_n \quad \text{(Equation S44)}$$

$$\dot{g}_n = x_n \quad \text{(Equation S45)}$$

since $z_{2n} = 0$.

For a finite time interval $[0, t_f]$ of interest, Equations (S44) and (S45) produce a unique solution $\bar{x}_n(t), \bar{g}_n(t)$ taking into account the initial conditions of the system. In addition, the origin is an exponentially stable equilibrium point of the boundary layer model:

$$\frac{dz_{2n}}{d\tau} = -z_{2n}$$

where $\tau = t_n/\lambda_1$.

Thus, according to Tikhonov's theorem (Theorem 11.1 in (Khalil, 2002)), there exist a positive constant λ_1^* such that for $0 < \lambda_1 < \lambda_1^*$ the singular perturbation problem of Equations (S40), (S41), and (S42) has a unique solution $x_n(t, \lambda_1), g_n(t, \lambda_1), z_{2n}(t, \lambda_1)$ on $[0, t_f]$ and

$$\begin{aligned}x_n(t, \lambda_1) - \bar{x}_n(t) &= \mathcal{O}(\lambda_1) \\ g_n(t, \lambda_1) - \bar{g}_n(t) &= \mathcal{O}(\lambda_1)\end{aligned}$$

Moreover, given any $t_b > 0$, there is λ_1^{**} such that

$$z_{2n}(t, \lambda_1) = \mathcal{O}(\lambda_1)$$

whenever $\lambda_1 < \lambda_1^{**}$.

Finally, combining Equations (S16), (S17), (S36), and (S37) results in:

$$\lambda_1 = \frac{Z_2^*}{Z_1^*}$$

Assuming that Z_1^* corresponds to some finite (nonzero) concentration, $Z_2^* \rightarrow 0$ as $\lambda_1 \rightarrow 0$.

Behavior analysis of biomolecular signal differentiators

Here we prove that, near their equilibria, BioSD networks are capable of signal differentiation.

We begin with BioSD-I whose dynamics close to its steady state are derived via linearization of [Equations \(S4\)](#) and [\(S5\)](#) as:

$$\begin{bmatrix} \dot{x} \\ \dot{z} \end{bmatrix} = \begin{bmatrix} \frac{k_2(k_{in}U^* + b)}{k_3} & \frac{k_1k_3}{k_2} \\ k_2 & 0 \end{bmatrix} \begin{bmatrix} x \\ z \end{bmatrix} + \begin{bmatrix} k_{in} \\ 0 \end{bmatrix} u \quad (\text{Equation S46})$$

assuming the coordinate transformations: $u = U - U^*$, $x = X - X^*$, $z = Z - Z^*$ which represent small perturbations around (U^*, X^*, Z^*) . Note that u represents U^{TV} of the main text. We next consider the non-dimensional variables:

$$t_n = c_1 t \quad (\text{Equation S47})$$

$$x_n = \frac{1}{c_3} x \quad (\text{Equation S48})$$

$$z_n = \frac{c_1}{k_2 c_3} z \quad (\text{Equation S49})$$

$$u_n = \frac{c_1 k_{in}}{k_2 c_2 c_3} u \quad (\text{Equation S50})$$

where

$$c_1 = \frac{k_2(k_{in}U^* + b)}{k_3} \quad (\text{Equation S51})$$

$$c_2 = \frac{k_1 k_3}{k_2} \quad (\text{Equation S52})$$

and c_3 is an arbitrary scaling parameter that carries the same units as x_n . We also introduce the non-dimensional parameter:

$$\varepsilon = \frac{c_1^2}{k_2 c_2} \quad (\text{Equation S53})$$

Substituting [Equations \(S47\)](#), [\(S48\)](#), [\(S49\)](#), [\(S50\)](#), [\(S51\)](#), [\(S52\)](#), and [\(S53\)](#) into the system [\(S46\)](#) results in:

$$\begin{aligned} \dot{x}_n &= -x_n - \frac{1}{\varepsilon} z_n + \frac{1}{\varepsilon} u_n \\ \dot{z}_n &= x_n \end{aligned}$$

or

$$\varepsilon \dot{x}_n = -\varepsilon x_n - z_n + u_n \quad (\text{Equation S54})$$

$$\dot{z}_n = x_n \quad (\text{Equation S55})$$

The system described by [Equations \(S54\)](#), [\(S55\)](#) is mathematically equivalent to the following second - order differential equation:

$$\varepsilon \ddot{x}_n + \varepsilon \dot{x}_n + x_n = \dot{u}_n \quad (\text{Equation S56})$$

We see immediately that if $\varepsilon(\ddot{x}_n + \dot{x}_n) = 0$ then $x_n = \dot{u}_n$ which gives through [Equations \(S47\)](#), [\(S48\)](#), [\(S50\)](#), and [\(S52\)](#):

$$x = \frac{k_{in}}{k_1 k_3} \dot{u} \quad (\text{Equation S57})$$

By recalling [Equation \(S6\)](#) and our initial coordinate transformations, this relationship can be rewritten as:

$$X = \frac{k_{in}}{k_1 k_3} \dot{U} + \frac{k_3}{k_2} \quad (\text{Equation S58})$$

Having this in mind and taking into account that ε is positive as a combination of positive parameters ([Equation \(S53\)](#)) we calculate the general solution of $\ddot{x}_n + \dot{x}_n = 0$ as:

$$x_n = \theta_1 e^{-t_n} + \theta_2 \quad (\text{Equation S59})$$

where θ_1, θ_2 are arbitrary constants. Subsequently, from [Equations \(S47\)](#), [\(S48\)](#), [\(S57\)](#), and [\(S59\)](#) we get:

$$u = f_1 e^{-c_1 t} + f_2 t + f_3 \quad (\text{Equation S60})$$

where f_1, f_2, f_3 are arbitrary constants.

To study the behavior of BioSD-I in the more general case where the input signal does not satisfy Equation (S60) we consider the following transfer function describing the system defined by Equations (S54) and (S54) in the Laplace domain:

$$\tilde{\Delta}_{\text{BSD}}(s) = \frac{\tilde{X}_n(s)}{\tilde{U}_n(s)} = \frac{s}{\varepsilon(s^2 + s) + 1} \quad (\text{Equation S61})$$

where $\tilde{X}_n(s)$ and $\tilde{U}_n(s)$ are the Laplace transform of the output x_n and input u_n , respectively and s is the complex frequency. As can be seen, BioSD-I can compute the derivative of the input signal filtered by a second-order low-pass filter.

As pointed out in Signals under consideration, Fourier transform is a powerful tool that allows the decomposition of a signal into its constituent sinusoids. Thus, focusing on the frequency response of the system, we set $s = j\omega$ (where $j = \sqrt{-1}$) in Equation (S61) to get:

$$\tilde{\Delta}_{\text{BSD}}(j\omega) = \frac{j\omega}{\varepsilon(-\omega^2 + j\omega) + 1} \quad (\text{Equation S62})$$

which can be equivalently represented by:

$$|\tilde{\Delta}_{\text{BSD}}(j\omega)| = \frac{\omega}{\sqrt{\varepsilon^2 \omega^2 + (1 - \varepsilon \omega^2)^2}} \quad (\text{Equation S63})$$

and

$$\angle \tilde{\Delta}_{\text{BSD}}(j\omega) = \arctan\left(\frac{1}{\varepsilon \omega} - \omega\right) \quad (\text{Equation S64})$$

As shown in Figure S3, for a given ε , there is a low-frequency range over which BioSD-I functions as a pure signal differentiator and, by extension Equation (S58) holds (the filtering action is practically zero), and a high-frequency one over which it works as a signal attenuator instead. At the same time, there is a narrow frequency band in between where the aforementioned operations may not be carried out with the expected accuracy. The behavior of BioSD-I therefore depends on the value of ε as well as on "how fast" an input signal varies over time.

Following the same procedure, we study the local dynamics of BioSD-III by linearizing Equations (S23), (S24), and (S25):

$$\begin{bmatrix} \dot{x} \\ \dot{z}_1 \\ \dot{z}_2 \end{bmatrix} = \begin{bmatrix} \frac{k_2(k_{in}U^* + b)}{k_3} & -\frac{k_1 k_3}{k_2} & \frac{k_1 k_3}{k_2} \\ k_2 & -\eta Z_2^* & -\eta Z_1^* \\ 0 & -\eta Z_2^* & -\eta Z_1^* \end{bmatrix} \begin{bmatrix} x \\ z_1 \\ z_2 \end{bmatrix} + \begin{bmatrix} k_{in} \\ 0 \\ 0 \end{bmatrix} u$$

where the variables $u = U - U^*$, $x = X - X^*$, $z_1 = Z_1 - Z_1^*$, $z_2 = Z_2 - Z_2^*$ refer to small perturbations around the equilibrium (U^*, X^*, Z_1^*, Z_2^*). Introducing the linear transformation $g = z_1 - z_2$ results in the following mathematically equivalent system:

$$\begin{bmatrix} \dot{x} \\ \dot{g} \\ \dot{z}_2 \end{bmatrix} = \begin{bmatrix} \frac{k_2(k_{in}U^* + b)}{k_3} & -\frac{k_1 k_3}{k_2} & 0 \\ k_2 & 0 & 0 \\ 0 & -\eta Z_2^* & -\eta(Z_1^* + Z_2^*) \end{bmatrix} \begin{bmatrix} x \\ g \\ z_2 \end{bmatrix} + \begin{bmatrix} k_{in} \\ 0 \\ 0 \end{bmatrix} u \quad (\text{Equation S65})$$

We notice that the dynamics of x and g of the system given by Equation (S65) are identical to that of x and z of the system given by Equation (S46), respectively. Hence, the output, x , of BioSD-III behaves in the exact same way as the one of previously analyzed BioSD-I.

Subsequently, we recall Equation (S30) describing the dynamics of BioSD-II near its equilibrium. It is evident that using the linear transformation $g = z_1 - z_2$ again and assuming a sufficiently large η (Equation (S43)

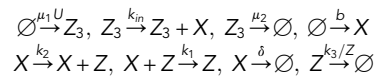
holds), the dynamics of x and g in BioSD-II are described by Equation (S46), namely the dynamics of BioSD-I (see The notion of strong rate of annihilation between Z_1, Z_2 (large η) in Biomolecular Signal Differentiator-II). By extension, the output behavior of these two circuits is identical.

An alternative version of biomolecular signal differentiators

Here we analyze a slightly different version of the previously studied BioSD networks which we call Biomolecular Signal Differentiators^F (BioSDs^F) that include an additional biomolecular species, Z_3 . In particular, we describe the following three biomolecular topologies:

- BioSD^F-I

We have the CRN:



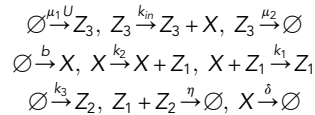
where $\mu_1, \mu_2, k_{in}, b, k_2, k_1, \delta, k_3 \in \mathbb{R}_+$. The 0th-order removal of Z is the result of enzymatic degradation following saturated Michaelis - Menten kinetics (see Equilibria and stability of biomolecular signal differentiators: biomolecular signal differentiator-I).

The corresponding ODE model is:

$$\begin{aligned} \dot{Z}_3 &= \mu_1 U - \mu_2 Z_3 \\ \dot{X} &= k_{in} Z_3 + b - k_1 X Z - \delta X \\ \dot{Z} &= k_2 X - k_3 \end{aligned}$$

- BioSD^F-II

We have the CRN:



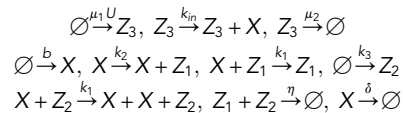
where $\mu_1, \mu_2, k_{in}, b, k_2, k_1, \delta, \eta \in \mathbb{R}_+$. We assume that the parameter rate η is sufficiently large (see The notion of strong rate of annihilation between Z_1, Z_2 (large η) in Biomolecular Signal Differentiator-II).

The corresponding ODE model is:

$$\begin{aligned} \dot{Z}_3 &= \mu_1 U - \mu_2 Z_3 \\ \dot{X} &= k_{in} Z_3 + b - k_1 X Z_1 - \delta X \\ \dot{Z}_1 &= k_2 X - \eta Z_1 Z_2 \\ \dot{Z}_2 &= k_3 - \eta Z_1 Z_2 \end{aligned}$$

- BioSD^F-III

We have the CRN:



where $\mu_1, \mu_2, k_{in}, b, k_2, k_1, \delta, \eta \in \mathbb{R}_+$.

The corresponding ODE model is:

$$\dot{Z}_3 = \mu_1 U - \mu_2 Z_3$$

$$\begin{aligned}\dot{X} &= k_m Z_3 + b - k_1 X Z_1 + k_1 X Z_2 - \delta X \\ \dot{Z}_1 &= k_2 X - \eta Z_1 Z_2 \\ \dot{Z}_2 &= k_3 - \eta Z_1 Z_2\end{aligned}$$

Each of the above circuits can be seen as the interconnection of two subsystems. More specifically, we have the linear, asymptotically stable, subsystem (the first equation in each of above ODE models):

$$\dot{Z}_3 = \mu_1 U - \mu_2 Z_3 \quad (\text{Equation S66})$$

which receives the signal U we want to differentiate as input and produces an output Z_3 . This is, in turn, applied as input to a second subsystem whose output is X . While the first subsystem is the same in all BioSD^F topologies, the second one differs. In fact, the latter is identical to BioSD-I, BioSD-II, BioSD-III (see previous sections) for BioSD^F-I, BioSD^F-II, BioSD^F-III, respectively, with the only difference lying in the input, which is now Z_3 (instead of U as before).

For a constant input U^* the first subsystem defined by Equation (S66) has a unique positive steady state (assuming it exists and is finite):

$$Z_3 = \frac{\mu_1 U^*}{\mu_2} \quad (\text{Equation S67})$$

Since Equation (S66) is linear and (μ_2) is always positive then Equation (S67) is a globally exponentially stable equilibrium point.

We now concentrate on the local behavior of BioSD^F modules and, consequently, we consider the coordinate transformations: $u = U - U^*$, $x = X - X^*$, $z = Z - Z^*$, $z_1 = Z_1 - Z_1^*$, $z_2 = Z_2 - Z_2^*$, $z_3 = Z_3 - Z_3^*$ denoting small perturbations around the corresponding equilibria of BioSD^F networks - (U^*, X^*, Z^*, Z_3^*) for BioSD^F-I and $(U^*, X^*, Z_1^*, Z_2^*, Z_3^*)$ for BioSD^F-II, BioSD^F-III (the steady states of the last two networks do not necessarily coincide).

First, we study Equation (S66) separately. In the Laplace domain, we have:

$$\tilde{\Delta}_{LPF}(s) = \frac{\tilde{Z}_3(s)}{\tilde{U}(s)} = \frac{\mu_1}{s + \mu_2} \quad (\text{Equation S68})$$

where $\tilde{Z}_3(s)$, $\tilde{U}(s)$ are the Laplace transform of z_3 , u , respectively. Focusing on the frequency response, we get:

$$\tilde{\Delta}_{LPF}(j\omega) = \frac{\mu_1}{\mu_2} \frac{1}{j\frac{\omega}{\mu_2} + 1} \quad (\text{Equation S69})$$

This is a transfer function of a first-order low-pass filter which is capable of preserving low-frequency signals and rejecting high-frequency signals. Indeed, the magnitude and the phase of the system in question are given by:

$$|\tilde{\Delta}_{LPF}(j\omega)| = \frac{\mu_1}{\mu_2} \frac{1}{\sqrt{1 + \left(\frac{\omega}{\mu_2}\right)^2}}$$

and

$$\angle \tilde{\Delta}_{LPF}(j\omega) = -\arctan \frac{\omega}{\mu_2},$$

respectively.

We can easily see that in practice, when $\omega \ll \mu_2$, there is a constant input/output gain $\left(\frac{\mu_1}{\mu_2}\right)$ and no phase lag. On the other hand, for $\omega^2 \gg \mu_2^2$ strong attenuation takes place. The general behavior of the filter can be easily understood through the Bode diagram in Figure S4.

We now consider a BioSD^F design which can be described by the transfer function of the series connection of the previously studied filter and a BioSD design (as already outlined in [Behavior analysis of biomolecular signal differentiators](#), all three BioSD circuits are described by the same transfer function), i.e.:

$$\tilde{\Delta}_{BDSDF}(s) = \frac{\tilde{X}_n(s)}{\tilde{U}_n(s)} = \tilde{\Delta}_{LPF}(s)\tilde{\Delta}_{BDS}(s)$$

or

$$\tilde{\Delta}_{BDSDF}(s) = \frac{\mu_1}{s + \mu_2} \cdot \frac{s}{\varepsilon(s^2 + s) + 1} \quad (\text{Equation S70})$$

where $\tilde{\Delta}_{LPF}(s) = \frac{\tilde{Z}_3(s)}{\tilde{U}_n(s)}$, $\tilde{\Delta}_{BDS}(s) = \frac{\tilde{X}_n(s)}{\tilde{Z}_{3n}(s)}$ with $\tilde{Z}_{3n}(s) = \rho\tilde{Z}_3(s)$ and $\rho = \frac{u_n}{u}$ (see [Behavior analysis of biomolecular signal differentiators](#)).

Shifting our focus on the frequency response we have:

$$\tilde{\Delta}_{BDSDF}(j\omega) = \tilde{\Delta}_{LPF}(j\omega)\tilde{\Delta}_{BDS}(j\omega) \quad (\text{Equation S71})$$

for which:

$$|\tilde{\Delta}_{BDSDF}(j\omega)| = |\tilde{\Delta}_{LPF}(j\omega)||\tilde{\Delta}_{BDS}(j\omega)|$$

and

$$\angle \tilde{\Delta}_{BDSDF}(\omega) = \angle \tilde{\Delta}_{LPF}(j\omega) + \angle \tilde{\Delta}_{BDS}(j\omega)$$

Consequently, for a given ε , BioSD^F circuits are characterized by an enhanced capability of high-frequency signal attenuation compared to BioSD ones. In fact, as demonstrated in [Figure S5](#), we can extend the frequency band where strong signal attenuation is carried out by appropriately tuning the filter module. In other words, we can adjust the bandwidth of the extra filter as desired through the parameter rate μ_2 . The price we pay for this significant improvement is the increase in structural complexity due to the addition of the species Z_3 via which the additional filtering is accomplished. Finally, in the low-frequency regime, where only signal differentiation takes place (the filtering action is practically zero), the BioSD^F output can be approximated in the time domain as (recall [Behavior Analysis of Biomolecular Signal Differentiators](#)):

$$X = \frac{\mu_1 k_{in} \dot{U} + k_3}{\mu_2 k_1 k_3 + k_2}$$

Analysis of the experimental topology of Biomolecular Signal Differentiator-III

Here we further analyze the proposed synthetic design of BioSD-III, the behavior of which may be more complicated due to the use of three auxiliary species (see [Guidelines for experimental implementation of biomolecular signal differentiators](#)).

The biomolecular topology shown in [Figure 8C](#) can be described by the following set of ODEs:

$$\dot{X} = k_{in}U + b - k_1XZ_1 + k_{1a}X_{aux}Z_{2,aux} - \delta X \quad (\text{Equation S72})$$

$$\dot{X}_{aux} = k_{in}U + b - k_{1b}X_{aux}Z_1 + k_{1a}X_{aux}Z_{2,aux} - \delta_a X_{aux} \quad (\text{Equation S73})$$

$$\dot{Z}_1 = k_2X - \eta Z_1 Z_2 \quad (\text{Equation S74})$$

$$\dot{Z}_{1,aux} = k_2X - \eta_a Z_{1,aux} Z_{2,aux} \quad (\text{Equation S75})$$

$$\dot{Z}_2 = k_3 - \eta Z_1 Z_2 \quad (\text{Equation S76})$$

$$\dot{Z}_{2,aux} = k_3 - \eta_a Z_{1,aux} Z_{2,aux} \quad (\text{Equation S77})$$

where k_{in} , b , k_2 , k_1 , k_{1a} , k_{1b} , δ , δ_a , η , $\eta_a \in \mathbb{R}_+$.

In order for the behavior of X (measured output species) in the system described by [Equations \(S72\)-\(S77\)](#) to perfectly match the one of X in the model given by [Equations \(S23\)-\(S25\)](#), we need: $k_1 = k_{1a} = k_{1b}$, $\delta = \delta_a$ and $\eta = \eta_a$. Nevertheless, non-satisfaction of the aforementioned conditions does not necessarily entail considerable loss of accuracy regarding signal differentiation ([Figure S6](#)).

Modeling a more realistic case of Biomolecular Signal Differentiator-II

Here we study the behavior of Biomolecular Signal Differentiator-II under more realistic conditions resulting from the corresponding experimental design discussed in [Guidelines for experimental implementation of biomolecular signal differentiators](#).

First, we consider the ODE model:

$$\dot{X} = k_{in}U + b - k_1XZ_1 - \delta X \quad (\text{Equation S78})$$

$$\dot{Z}_1 = V_{max} \frac{X}{X + K_m} - \eta Z_1 Z_2 \quad (\text{Equation S79})$$

$$\dot{Z}_2 = k_3 - \eta Z_1 Z_2 \quad (\text{Equation S80})$$

For a constant input U^* , provided that:

$$(k_{in}U^* + b) > \delta X^*,$$

we have a unique positive (finite) steady state:

$$X^* = \frac{k_3 K_m}{V_{max} - k_3} \quad (\text{Equation S81})$$

$$Z_1^* = \frac{(k_{in}U^* + b) - \delta}{k_1 X^*} \quad (\text{Equation S82})$$

$$Z_2^* = \frac{k_3}{\eta Z_1^*} \quad (\text{Equation S83})$$

Compared to the original model of BioSD-II ([Equations \(S11\), \(S12\), and \(S13\)](#)), we now use a Michaelis-Menten function to describe the activation of species Z_1 by species X ([Equation S79](#)) through gene expression ([Aoki et al., 2019](#)). It is evident that, assuming small perturbations around (U^*, X^*, Z_1^*, Z_2^*) , linearization of [Equations \(S78\), \(S79\), and \(S80\)](#) yields a system of the same form as [Equation \(S30\)](#). Consequently, we can follow a similar analysis to study its local behavior as the one used for the original model (see [The notion of strong rate of annihilation between \$Z_1, Z_2\$ \(large \$\eta\$ \) in biomolecular signal differentiator-II and Behavior analysis of biomolecular signal differentiators](#)). Nevertheless, it should be emphasized that when no saturation occurs and the slope of the Michaelis-Menten function is approximately linear, the corresponding production rate can be effectively considered proportional to the concentration of the regulator species (*ibid.*). In that case, the results of our original analysis can be used directly.

Implementation of BioSD-II in living cells implies the existence of an additional degradation mechanism due to cell growth affecting all the biomolecules involved, known as dilution ([Aoki et al., 2019; Qian and Del Vecchio, 2018](#)). This can lead to a “leaky” integration process realized by species Z_1, Z_2 and, by extension, it can affect the output response (see [Achieving biological signal differentiation](#)). To this end, we consider the following, more complex, ODE model:

$$\dot{X} = k_{in}U + b - k_1XZ_1 - (\delta + \gamma)X \quad (\text{Equation S84})$$

$$\dot{Z}_1 = V_{max} \frac{X}{X + K_m} - \eta Z_1 Z_2 - \gamma Z_1 \quad (\text{Equation S85})$$

$$\dot{Z}_2 = k_3 - \eta Z_1 Z_2 - \gamma Z_2 \quad (\text{Equation S86})$$

where γ represents a dilution rate constant.

In general, linearization of [Equations \(S84\), \(S85\), and \(S86\)](#) around their steady-state (which is obviously different than before) results in a system which does not have the same form as [Equation \(S30\)](#) and, thus, the procedures of our original analysis are not valid here. Nevertheless, if the dilution effect is not strong, it can be seen from simulations that the behavior of this model approaches the one of [Equations \(S78\), \(S79\), and \(S80\)](#).

Note that the above structural “perturbations” appear also in the natural systems discussed in [Biomolecular signal differentiators in natural regulatory networks](#). In parallel, activation of species X by Z and Z_1 in BioSD-I and BioSD-III, respectively is also done through gene expression (see [Guidelines for experimental implementation of biomolecular signal differentiators](#)). In addition, dilution is present when realizing the latter topologies in living cells. Consequently, we can draw similar conclusions about them as with BioSD-II.

We now numerically investigate the behavior of BioSD-II. Figure S7A shows the response of the system given by Equations (S78), (S79), and (S80) to the input presented in Figure 3C using the parameter rates in Table S1, except for the dilution rate γ which is considered zero. As can be seen, BioSD-II can accurately calculate the rate of change of the input applied.

Note also the following:

- From Equation (S85) and Table S1 we calculate the steady-state concentration of species X which is equal to 20 nM. Based on the values of V_{max} , K_m and taking into account that X moves around the aforementioned point, the production rate of species Z₁ can be approximated well by the term k_2X , where $k_2 \approx 1$ (no saturation occurs).
- To facilitate the comparison of the BioSD output with the derivative of the input we choose a value for k_{in} equal to the value of the quantity k_1k_3 (see Equation (S58)). At the same time, here input U represents an actuator species whose concentration is related linearly with the corresponding production rate of output species X (which may result from the linear regime of a Hill function as discussed above). Nevertheless, in the general case the term $k_{in}U$ can represent any (nonlinear) function describing the activating mechanism of the output species.
- From Equation (S53) we get $\epsilon \approx 0.125$. Moreover, η can be considered sufficiently large since $\eta = 425 \text{ nM}^{-1} \text{ min}^{-1} \gg \frac{\beta_1^2}{k_3} \approx 14.18 \text{ nM}^{-1} \text{ min}^{-1}$ (see Equation (S36)). Consequently, Equation (S43) holds.
- Protein production rates regarding gene expression can be easily adjusted, for example, by changing gene copy number and, thus, a wide range of values can be achieved - a typical parameter range for *E. coli* is $0.5 - 10^4 \text{ nM nM}$ (Aoki et al., 2019). This implies extensive tunability which is important for meeting different performance standards (see Tunability and accuracy) since a considerable number of parameter rates in BioSD-II is associated with gene expression, i.e. b , k_2 (which is related to V_{max} , K_m), k_3 and k_{in} .

Figure S7B shows the response of the system given by Equations (S84), (S85), and (S86) to the same input stimulus. We also use the same parameters rates as before except for the dilution rate which is now nonzero and equal to a typical value for *E. coli* (see Table S1). It is evident that the output remains an accurate replica of the derivative of the input.

Subsequently, in Figures S7C and S7D we further investigate the impact of dilution on the output of BioSD-II by repeating the simulation of Figure S7B with a 5 and 10 times larger dilution rate, respectively. We notice that as this rate gets stronger the actual response moves away from the zero-level "bias" which coincides with the corresponding output steady-state. Moreover, although the accuracy drops to some extent, the form of the output remains close to the one of the ideal derivative.

As already pointed out, the annihilation rate η is chosen to be sufficiently large so that the condition given by Equation (S43) is satisfied (only BioSD-II entails such a requirement). More specifically, η is approximately 30 times larger than the quantity $\frac{\beta_1^2}{k_3}$. Nevertheless, it remains unclear to us if such suitable values of η can be always guaranteed *in vitro* by the interaction between the pair of protease/protease inhibitor proposed in Guidelines for experimental implementation of biomolecular signal differentiators. It is therefore important to investigate the behavior of the differentiator module in the case where η is not as large as our theoretical analysis demands. As shown in Figure S8, non-satisfaction of the condition given by Equation (S43) does not necessarily entail significant loss of accuracy regarding signal differentiation. Note also that the quantity $\frac{\beta_1^2}{k_3}$ can be easily adjusted to a suitable value by appropriately tuning the protein production rates involved in BioSD-II (discussed earlier).

Finally, to make the above analysis even more realistic (Del Vecchio and Murray, 2015), one could model gene expression as a multi-stage process, thus capturing the dynamics of transcription and translation. At the same time, the dynamics of complexes participating in intermediate stages of inhibition and annihilation reactions could also be considered. Nonetheless, it is important to emphasize that such an approach would increase the complexity of the resulting mathematical models.